Chemical Compatibilization, Macro-, and Microphase Separation of Hetero-Associative Polymers

Scott P. O. Danielsen*

NSF Center for the Chemistry of Molecularly Optimized Networks, Soft Matter Center, and Thomas Lord Department of Mechanical Engineering and Materials Science, Duke University, Durham, NC 27708, United States

E-mail: scott.danielsen@duke.edu

For Table of Contents use only

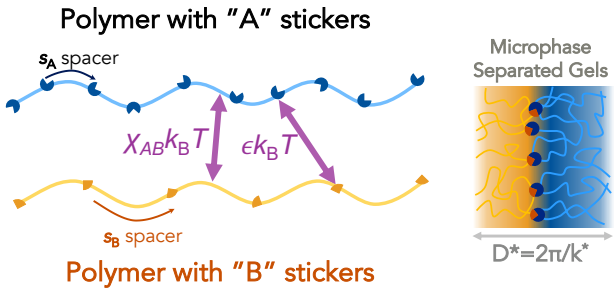

Abstract

A mean-field equilibrium theory for reversible network formation due to heterotypic pairwise interactions in mixtures of associative polymers is extended via a weak inhomogeneity expansion to account for spatial fluctuations due to chemical incompatibility. We consider solutions and blends of polymers of types A and B with many associating groups per chain, and consider only $A-B$ association between these groups. The structural correlations of the reversibly-bonded polymers are accounted for by considering the Gaussian 4-arm star-like chain conformations between cross-links, which is analogous to an affine-network assumption. Future extensions of this theory could further incorporate strand stretching from swelling or strong segregation. We show that the chemical incompatibility between A and B polymers drives a competition between associative and segregative phase separation. The addition of reversible $A-B$ cross-links between incompatible A and B chains compatibilizes the mixture, minimizing the propensity for macroscopic phase separation into A- and B-rich phases. Under strong binding and segregation conditions, this results in eutectic-like behavior and local microphase segregation. The crossovers from macroscopic to microscopic phase separation occur at isotropic Lifshitz points, resulting in the potential for bicontinuous microemulsions. The reactive blending of such multifunctional polymers presents the opportunity to envision novel properties, processing conditions, and applications accessible by the tunable production of supramolecular complexes, mesophases, and multicomponent polymer networks.

Introduction

Blending polymer melts or solutions into a polymeric alloy is a straightforward and important approach for designing high-performance materials.[1] Polymer blends allow material properties to be optimized due to the combination of exceptional properties from multiple constituents. However, segregation effects arising from chemical incompatibility between the polymers often hinder their utility.

Polymer mixtures tend to phase separate, as their translational entropy is small for long chains, considerably amplifying the chemical mismatch between unlike monomers. Segregation occurs below a critical temperature (i.e., above a critical strength of interaction), resulting in poor-quality materials with weak interfaces and limited control over their morphology or properties.[1–3] Since the size and microstructure of the phase-segregated domains dictate the macroscopic properties of the material, controlling separation on prescribed length scales, however, enables tailoring of the material.

A simple approach for enhancing miscibility in a polymer blend is to prevent coarsening of the macroscopic coexisting phases. Accordingly, one method is to create bonds between different chemical species, chemically cross-linking the mixture in the one-phase region or early in the phase separation process.[4–8] Cross-linking reactions permit the formation of quenched domains in the range of nanometers to micrometers. Properties such as the optical transparency and mechanical behavior depend on the size of the composite domains, which can be controlled by the degree of cross-linking (i.e., distance between cross-links) and the length scale of concentration fluctuations in both the preparation and use conditions.[7–10]

Another approach arrests phase separation by the inclusion of an appropriate compatibilizer, often a block, random, or graft copolymer. These additives preferentially adsorb to the interfaces between A and B domains, serving to lower the interfacial tension, forming a finer dispersion, strengthening the polymer alloy and stabilizing complex morphologies.[11–15]

Recently, reactive blending technologies have offered an integrated approach by forming compatibilizers in situ directly at the blend interface.[15–20] Mutually reactive ($A-B$) polymers

are blended, reactions at the interface form block copolymer "surfactants", promoting mixing and subsequently superior material properties. Interestingly, when bonding conditions are favorable, the resultant copolymers produced in the blend can form ordered mesophases that can drastically affect the overall material's structure and properties.[20–24]

Reactive blending relies on the binding of A chains to B chains at the interface. Typically, this is achieved by reactive sites at the chain ends, which can form covalent bonds with the other blend components. Practically, however, reversible bonds between associative groups, or "stickers", offer a more facile and tunable approach for in situ compatibilizer formation. Because the objective is selective binding between A and B chains, hetero-complementary (or heterotypic or heteroleptic) associations, in which an A reactive group binds to a B reactive group, are preferred. Such heterotypic attractive associations can include hydrogen bonding, metal–ligand, cation–π, host–guest, or ionic interactions.[20,25–28]

The physical bonds improve the mutual miscibility between different species but also result in complex phase behavior, including macro- and microscopic phase separation, as well as gel formation. The size, morphology, and connectivity of the resultant material structures critically depend on the interplay between the strength of these physical reversible associations and the chemical incompatibility driving segregation.[10,29–31]

The extension of reactive blending to multifunctional polymers with many associating groups per chain creates the opportunity to envision novel properties, processing conditions, and applications accessible by the tunable production of supramolecular complexes, mesophases, and multicomponent polymer networks in these systems. Such materials should be self-healing or remendable, able to re-gain their structure and properties after failure.[32–36] In fact, comparable systems already exist in nature, with transient associations between proteins and nucleic acids driving sub-cellular and nuclear compartmentalization important in membraneless organelles and chromatin transcription.[37–42]

Clearly, there is an immense parameter space possible in associating polymer mixtures: polymer architecture and molecular weight, solvent quality, chemical incompatibility be-

tween different species, sticker density and sequence, and binding strength of the associations. The vast potential of the property space and the complexity of the design space motivate a theoretical foundation for robust design principles that link the thermodynamics, gelation, and resulting properties of these materials.[29–31,35,43–55] In a companion work, we developed a mean-field theory for the thermodynamics and gelation of two-component solutions of *heterotypic* or $A-B$-type associative polymers.[47] Reversible binding between hetero-complementary associating groups were found to result in branched copolymers and macroscopic percolation. Homogeneous networks are most easily stabilized near stoichiometric sticker conditions, enabling sol–gel–sol transitions as the overall composition of the mixture is altered. Good solvent conditions reduce the associations between chains, suppressing phase separation, as for *homotypic* or $A-A$-type sticky polymers.[46] However, existing mean-field theories are restricted to spatially homogeneous networks and are therefore not suitable for addressing questions of microphase segregation.

In this study, we investigate with a minimal theory the phase separation and gelation of a mixture of reversibly bonded multifunctional associating polymers of types A and B. The reversible bonding of hetero-associating groups transforms the polymer blends into macroscopic copolymer networks. Gelation proceeds when the reversible network achieves percolation across the sample, with an average of two cross-links per chain.[47] By extension of an equilibrium mean-field theory to account for spatial concentration fluctuations, we can furthermore describe the competition between chemical incompatibility and reversible binding that leads to macro- and microphase separation. The described polymer alloys have the advantage of thermal tuning of connectivity and segregation strength, leading to controllable phase behavior and network formation, with implications for biological condensates and polymer reprocessing.

Theory

Mean-Field Model

We consider a mixture of multifunctional polymers consisting of linear chains with associating groups of type $i = A, B$ (Figure 1).[47] The polymers have N_i segments of size a and have ideal chain statistics described by the continuous Gaussian chain model. Each chain contains f_i stickers separated by spacers with $s_i = N_i/(f_i - 1)$ segments. There are many stickers per chain, but significantly fewer than the number of Kuhn segments ($1 \ll f_i \ll N_i$) such that the spacers between stickers are long ($s_i \gg 1$) and the effects of sticker cooperativity can be neglected. Stickers can associate in saturable, heterotypic (i.e., heteroleptic or hetero-bonding, only $A - B$, not $A - A$ or $B - B$) pairs with the energy of each bond equal to $\epsilon\, k_\mathrm{B}T$, where $k_\mathrm{B}T$ is the thermal energy.

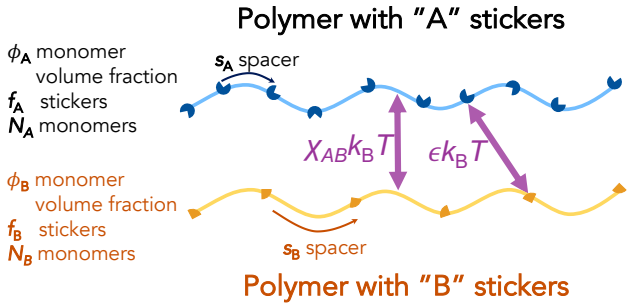

Figure 1: Model system of $A - B$ associative polymers.

The monomer volume fraction of type i in solution is ϕ_i, the number density of polymer chains is $\phi_i/(a^3 N_i)$, and the number density of stickers is $f_i\phi_i/(a^3 N_i) \simeq \phi_i/(a^3 s_i)$. The degree of conversion of type $i = A, B$, p_i, is the fraction of stickers of type i that are associated in a bound $A - B$ pair. The average number density of reversible bonds is

$$\rho = p_i \frac{f_i \phi_i}{a^3 N_i} \simeq p_i \frac{\phi_i}{a^3 s_i} \tag{1}$$

where we have defined the concentration from the volume fractions and segmental volume

a^3. The total volume fraction $\phi = \phi_A + \phi_B$ is equal to unity in the limit of an incompressible melt blend and less than unity when suspended in solvent.

Weak Inhomogeneity Expansion

If the system undergoes local fluctuations, ϕ_A and ϕ_B become space dependent, and the resulting free energy functional becomes

$$F\{\phi_A(\mathbf{r}), \phi_B(\mathbf{r})\} = F_{\text{tr}} + F_{\text{int}} + F_{\text{st}} \tag{2}$$

with the resulting formalism suitable for both homogeneous and inhomogeneous phases. The first term F_{tr} accounts for the translational entropy of the chains:

$$\frac{F_{\text{tr}}}{k_{\text{B}}T} = \int d^3\mathbf{r} \left[\frac{\phi_A(\mathbf{r})}{N_A} \ln\left(\phi_A(\mathbf{r})\right) + \frac{\phi_B(\mathbf{r})}{N_B} \ln\left(\phi_B(\mathbf{r})\right) \right] \tag{3}$$

The second term F_{int} captures the solvent-mediated excluded volume interactions between monomers and $A - B$ chemical incompatibility:

$$\frac{F_{\text{int}}}{k_{\text{B}}T} = \int d^3\mathbf{r} \left[\frac{v}{2}(\phi_A(\mathbf{r}) + \phi_B(\mathbf{r}))^2 + \frac{w}{6}(\phi_A(\mathbf{r}) + \phi_B(\mathbf{r}))^3 + \chi_{AB}\phi_A(\mathbf{r})\phi_B(\mathbf{r}) \right] \tag{4}$$

where v is the excluded volume parameter, w is the three-body interaction parameter, and χ_{AB} is the Flory–Huggins parameter between the A and B polymers relative to the solvent. We assert in this analysis that v, w, and χ_{AB} are not directly affected by the presence of cross-links and that the solvent is of equal quality for both A and B (i.e., $v_A = v_B \equiv v$ and $w_A = w_B \equiv w$). For simplicity and consistency with Ref. 47, we will set $v = 0$ and $w = 1$ to approximate Θ-solvent or nearly incompressible melt conditions. However, it should be noted that other choices for v and w are allowed in this framework and might be more suitable for compressible melts as in the Helfand description. Finally, the last term in eq. 2

is responsible for the enthalpy of sticker bonds and combinatorial entropy of stickers,[47,56,57]

$$\frac{F_{\mathrm{st}}}{k_{\mathrm{B}}T} = \int d^3\mathbf{r} \left[\frac{\phi_A(\mathbf{r})}{s_A} \left[p_A(\mathbf{r}) + \ln\left(1 - p_A(\mathbf{r})\right) \right] + \frac{\phi_B(\mathbf{r})}{s_B} \ln\left(1 - p_B(\mathbf{r})\right) \right] \tag{5}$$

where, importantly, the degrees of conversion of stickers $p_A(\mathbf{r})$ and $p_B(\mathbf{r})$ are also spatially-dependent functions. The bond strength ϵ enters this sticker energy implicitly through the degrees of conversion of A and B. This description of pairwise association between hetero-complementary stickers concurs with previous works on ion pair formation in polyelectrolytes.[57–61] Minimization of the free energy (eq. 2) with respect to the number density of sticker bonds $\rho a^3 = p_A\phi_A/s_A = p_B\phi_B/s_B$ results in an expression for the degree of conversion of A stickers:[47]

$$p_A(\mathbf{r}) = \frac{1}{2} + \frac{\phi_B(\mathbf{r})/s_B}{2\phi_A(\mathbf{r})/s_A} + \frac{1 - \sqrt{\left(1 + \left(\frac{\phi_A(\mathbf{r})}{s_A} + \frac{\phi_B(\mathbf{r})}{s_B}\right)\lambda\right)^2 - 4\frac{\phi_A(\mathbf{r})}{s_A}\frac{\phi_B(\mathbf{r})}{s_B}\lambda^2}}{\frac{2\phi_A(\mathbf{r})}{s_A}\lambda} \tag{6}$$

where $\lambda = (v_{\mathrm{b}}/a^3)\exp(\epsilon)$ is the attractive volume of a bond (relative to segmental volume a^3), an exponential of the association strength. The degree of conversion of B stickers is related to the degree of conversion of A stickers by the relative concentrations of stickers of A and B: $p_B(\mathbf{r})/p_A(\mathbf{r}) = (\phi_A(\mathbf{r})/s_A)/(\phi_B(\mathbf{r})/s_B) = r(\mathbf{r})$, where r is the sticker stoichiometry. For spatially homogeneous systems, the gelation condition corresponds to the degrees of conversion of A and B,[30,47,51,62–66]

$$p_A^{\mathrm{gel}} p_B^{\mathrm{gel}} = r p_A^{\mathrm{gel}\,2} = \frac{1}{f_A - 1}\frac{1}{f_B - 1} \tag{7}$$

where the superscript "gel" refers to the critical fractional conversions at the gel point.

We can assess the stability limit of the homogeneous phase via a weak inhomogeneity expansion (the so-called random phase approximation, RPA.)[67,68] Thus, we consider weak

spatially varying concentration perturbations of the form

$$\phi_i(\mathbf{r}) = \phi_i + \sigma\delta_i(\mathbf{r}) \tag{8}$$

where ϕ_i is the mean value of the concentration given by

$$\phi_i = \frac{1}{V}\int d^3\mathbf{r}\,\phi_i(\mathbf{r}) \tag{9}$$

and σ is a positive constant such that $\sigma \ll 1$ and $\delta_i(\mathbf{r})$ is the spatially varying part of the concentration. Substituting the concentration perturbations (eq. 8) into the free energy functional (eq. 2) and expanding into a series of small fluctuations $\delta_i(\mathbf{r})$, we can decompose the free energy density into mean-field and fluctuation correction contributions:

$$\frac{F}{Vk_{\mathrm{B}}T} = \frac{F_0}{Vk_{\mathrm{B}}T} + \frac{1}{2V}\int d^3\mathbf{r}\,\frac{F^{\mathrm{fluct}}}{k_{\mathrm{B}}T}(\delta_A(\mathbf{r}),\delta_B(\mathbf{r})) + \cdots \tag{10}$$

where the mean-field part of the free energy described by uniform (average) compositions is[47]

$$\frac{F_0}{Vk_{\mathrm{B}}T} = \frac{\phi_A}{N_A}\ln(\phi_A) + \frac{\phi_B}{N_B}\ln(\phi_B) + \frac{v}{2}(\phi_A+\phi_B)^2 + \frac{w}{6}(\phi_A+\phi_B)^3 + \chi_{AB}\phi_A\phi_B + \frac{\phi_A}{s_A}[p_A + \ln(1-p_A)] + \frac{\phi_B}{s_B}\ln(1-p_B) \tag{11}$$

The deviation of the local monomer volume fraction from its average, $\delta_i(\mathbf{r})$, serves as a characteristic order parameter, which is zero in the disordered, homogeneous state and finite otherwise. It proves convenient to use Fourier transformations to provide factorization of fluctuations with different wave vectors $\mathbf{k}$ and represent the fluctuation-induced variation of the free energy (truncated at the leading term in the δ_i series expansion) as

$$\frac{F}{Vk_{\mathrm{B}}T} = \frac{F_0}{Vk_{\mathrm{B}}T} + \frac{a^3}{2}\int \frac{d^3\mathbf{k}}{(2\pi)^3}\mathbf{S}^{-1}(\mathbf{k})\delta_j(\mathbf{k})\delta_l(-\mathbf{k}) \tag{12}$$

with $j, l = A, B$. The kernel in eq. 12 is the inverse structure factor matrix

$$\mathbf{S}^{-1}(\mathbf{k}) = \mathbf{S}_0^{-1}(\mathbf{k}) + \mathbf{U}(\mathbf{k}) \tag{13}$$

and in the random phase approximation can be separated into inverse intra-chain $\mathbf{S}_0^{-1}(\mathbf{k})$ and interaction $\mathbf{U}(\mathbf{k})$ contributions.[69–72] The interaction matrix has components:

$$U_{AA} = v + w(\phi_A + \phi_B) + \frac{1}{s_A^2}\left(\frac{1 + \left(\frac{\phi_A}{s_A} + \frac{\phi_B}{s_B}\right)\lambda}{2\frac{\phi_A}{s_A}\sqrt{1 + 2\left(\frac{\phi_A}{s_A} + \frac{\phi_B}{s_B}\right)\lambda + \left(\frac{\phi_A}{s_A} - \frac{\phi_B}{s_B}\right)^2\lambda^2}} - \frac{1}{2\frac{\phi_A}{s_A}}\right) \tag{14}$$

$$U_{BB} = v + w(\phi_A + \phi_B) + \frac{1}{s_B^2}\left(\frac{1 + \left(\frac{\phi_A}{s_A} + \frac{\phi_B}{s_B}\right)\lambda}{2\frac{\phi_B}{s_B}\sqrt{1 + 2\left(\frac{\phi_A}{s_A} + \frac{\phi_B}{s_B}\right)\lambda + \left(\frac{\phi_A}{s_A} - \frac{\phi_B}{s_B}\right)^2\lambda^2}} - \frac{1}{2\frac{\phi_B}{s_B}}\right) \tag{15}$$

$$U_{AB} = U_{BA} = v + w(\phi_A + \phi_B) + \chi_{AB} - \frac{1}{s_A s_B}\left(\frac{\lambda}{\sqrt{1 + 2\left(\frac{\phi_A}{s_A} + \frac{\phi_B}{s_B}\right)\lambda + \left(\frac{\phi_A}{s_A} - \frac{\phi_B}{s_B}\right)^2\lambda^2}}\right) \tag{16}$$

which balance short-range repulsions with sticker–sticker attractions. The repulsions add to the excess free energy of interaction and are positive, while the attractions reduce the free energy of interaction, subtracting from U_{AB}. The final terms of each interaction matrix component U_{ij} representing the sticker interactions can be recast in the average degrees of conversion of A and B, p_A and $p_B = rp_A$, resulting in

$$U_{AA} = v + w(\phi_A + \phi_B) + \frac{1}{\phi_A s_A}\left(\frac{p_A p_B}{1 - p_A p_B}\right) \tag{17}$$

$$U_{BB} = v + w(\phi_A + \phi_B) + \frac{1}{\phi_B s_B}\left(\frac{p_A p_B}{1 - p_A p_B}\right) \tag{18}$$

$$U_{AB} = U_{BA} = v + w(\phi_A + \phi_B) + \chi_{AB} - \frac{1}{\phi_A s_B}\left(\frac{p_B}{1 - p_A p_B}\right) \tag{19}$$

which emphasizes the thermodynamic consequences of pairwise hetero-association, evidenced

by interactions dependent on the product $p_A p_B$. Importantly, the sign of the sticker interaction term is positive for $A-A$ and $B-B$ self-interactions (i.e., repulsive), but negative and, thus attractive, for $A-B$ cross-interactions. Prior works have introduced the concept of an effective chi,[58,73] χ_{AB}^{eff}, that smears out all interactions into a single effective parameter:

$$\chi_{AB}^{\text{eff}} = U_{AB} - (U_{AA} + U_{BB})/2 \tag{20}$$

$$= \chi_{AB} - \frac{p_A p_B(\phi_A s_A + \phi_B s_B) - p_A \phi_A s_B - p_B \phi_B s_A}{2(1 - p_A p_B)\phi_A \phi_B s_A s_B} \tag{21}$$

in which increasing associations lower the bare chi parameter, i.e., compatibilization. However, in the present work, we not only account for associations in $\mathbf{U}(\mathbf{k})$, but also in how they affect the chain correlations.

Rigorously, the connectivity of each polymeric species must be accounted for explicitly in the intramolecular correlation matrix $\mathbf{S}_0(\mathbf{k})$. However, unlike simpler supramolecular or telechelic models in which generating functions provide a useful approximation,[74–77] an unlimited number of species are formed by the association of multifunctional polymers that cannot be enumerated. In principle, this case is well suited to the use of the coherent states formalism of polymer field theory,[49,78] which is theoretically capable of specifying all possible reaction products, but the numerical implementation of such models is currently challenging.[49]

Here, we account for the Gaussian chain structure of un-associated chains of A and B and describe the associated chain configurations as an effective A_2B_2 4-arm star copolymer with two arms of $n_A/2$ A monomers and two arms of $n_B/2$ B monomers around each reticulation site (Fig. 2).[28,79,80] This amounts to an affine network approximation and should be most applicable at high polymer concentration and association strength conditions. Consequently, we neglect cyclic[81–83] and higher-order branched species.

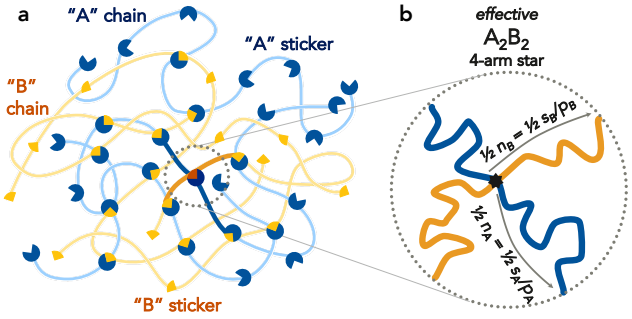

Figure 2: (a) Schematic illustration of reversibly bonded mixture of A and B chains. (b) Effective A_2B_2 4-arm star structure of $A-B$ associative polymers used in developing correlation functions.

Within this approximation, the intramolecular correlation matrix $\mathbf{S}_0(\mathbf{k})$ has components:

$$\begin{aligned} S_{0,AA} &= \mathrm{H}(s_A/p_A - N_A)(\phi_A/N_A - p_A\phi_A/s_A)\mathrm{g_D}(N_A,k) \\ &\quad + 2(p_A\phi_A/s_A)\left[\mathrm{g_D}(n_A/2,k) + \mathrm{h_D}^2(n_A/2,k)\right] \end{aligned} \tag{22}$$

$$\begin{aligned} S_{0,BB} &= \mathrm{H}(s_B/p_B - N_B)(\phi_B/N_B - p_B\phi_B/s_B)\mathrm{g_D}(N_B,k) \\ &\quad + 2(p_B\phi_B/s_B)\left[\mathrm{g_D}(n_B/2,k) + \mathrm{h_D}^2(n_B/2,k)\right] \end{aligned} \tag{23}$$

$$\begin{aligned} S_{0,AB} &= 4(p_A\phi_A/s_A)\mathrm{h_D}(n_A/2,k)\mathrm{h_D}(n_B/2,k) \\ &= 4(p_B\phi_B/s_B)\mathrm{h_D}(n_A/2,k)\mathrm{h_D}(n_B/2,k) = S_{0,BA} \end{aligned} \tag{24}$$

where $\mathrm{H}(x)$ is the Heaviside step function. The correlations are constructed from the Debye function,

$$\mathrm{g_D}(n,k) = \frac{2}{(k^2a^2/6)^2}\left[e^{-nk^2a^2/6} + nk^2a^2/6 - 1\right] \tag{25}$$

and a partial Debye-like function

$$\mathrm{h_D}(n,k) = \frac{1}{(k^2a^2/6)}\left[1 - e^{-nk^2a^2/6}\right] \tag{26}$$

that depend on the wave number $k = |\mathbf{k}|$ and the strand sizes n.[67] The average strand lengths between cross-links of type $i = A, B$

$$n_i = \begin{cases} N_i & \text{for } s_i/p_i \geq N_i \\ s_i/p_i & \text{for } s_i/p_i < N_i \end{cases} \tag{27}$$

are functions of the degrees of conversion of stickers. At high degrees of association, the average strand length between paired stickers n_i approaches the average number of segments between stickers s_i; but, at low conversion, n_i is bound by the degrees of polymerization N_i of the initial linear polymers. The Heaviside step function $H(x)$ enters into eqs. 22-23 to enforce the transition from unreacted linear chains without associated stickers to effective star-like copolymers with one or more cross-links. For $s_i/p_i \geq N_i$, the initially formed star-like polymers are limited to strand lengths of $n_i = N_i$, prior to further associations reducing $n_i < N_i$. In the limit of $p_A, p_B \to 0$, $\mathbf{S}_0(\mathbf{k})$ reduces to that of a binary mixture of linear homopolymers of type A and B with degrees of polymerization N_i; in the limit of $p_A, p_B \to 1$, $\mathbf{S}_0(\mathbf{k})$ reduces to that of a solution of A_2B_2 4-arm stars with arm degrees of polymerization $s_i/2$. In calculating the correlation functions, we have assumed that the spatial distribution of each block in a multicomponent copolymer obeys Gaussian statistics (recall the use of the Debye function in eqs. 22-24). The assumption breaks down if the blocks are very short (i.e., the distance between cross-links is of order of the persistence length, $s_i/p_i \not\gg 1$). Although exceptionally crude, we will see that these approximations are sufficient to qualitatively capture the physics of multifunctional associative polymer mixtures.

It is useful to compare this framework with the seminal work by de Gennes on irreversibly cross-linked blends of A and B polymers, where, in an analogy to dielectric polarization, he defined an internal rigidity constant $\sim n^{-2}$ to capture the elastic contribution of strands of n monomers between cross-links resisting phase separation.[7] From the free energy functional defined above, eq. 12, a Taylor expansion in k produces an analogous $\mathcal{O}(k^{-2})$ term, with

coefficient:

$$\frac{36}{\rho}\frac{p_A}{s_A}\frac{p_B}{s_B}\left(\frac{p_A}{s_A}+\frac{p_B}{s_B}\right)=\frac{36rp_A^2}{s_As_B}\left(\frac{1}{\phi_A}+\frac{1}{\phi_B}\right) \tag{28}$$

where p_A and p_B are the average degrees of conversion of A and B stickers. This coefficient is a direct result of the bare correlation functions constructed for the "effective" star polymers constituting the network (Figure 2), which introduced k-dependence. The exact numerical prefactor is dependent on our choices regarding a 4-arm star (as compared to linear diblock or more complex architectures.)

However, we can interpret this coefficient in the same context as de Gennes' phenomenological internal rigidity constant.[7] It increases with decreasing concentration and is inversely proportional to the square of the number of monomers between cross-links, as predicted for the case of permanent networks.[7,84–86] Importantly, this internal rigidity characterizing the elasticity is also highly sensitive to the asymmetry in the concentrations of stickers A and B (directly and implicitly through p_A), emphasizing the strong effects of sticker mismatch[47] and spatial inhomogeneity.[87] Furthermore, the elastic constant is proportional to the product of the degrees of conversion of stickers A and B, a consequence of the hetero-binding conditions.[47] As such, the rigidity constant depends on the fractional conversion of binding as was asserted for permanent networks.[84–86]

The homogeneous mixture is unstable to fluctuations when $\mathbf{S}^{-1}(\mathbf{k})$ is not positive definite. The spinodal condition can then be determined according to $\det[\mathbf{S}^{-1}(\mathbf{k})] = \det[\mathbf{S}_0^{-1}(\mathbf{k}) + \mathbf{U}(\mathbf{k})] = 0$. The stability limit equivalently corresponds to a divergence in the scattering function $S(k^*) \to \infty$ at a critical value of the wave number $k = k^*$. Phase separation proceeds macroscopically into two homogeneous phases if the scattering function diverges at $k = 0$ or into an ordered microphase with periodicity $D^* = 2\pi/k^*$ if $S(k)$ diverges at a finite value of k^*.

While the theory is applicable across the spectrum of binding energies, since heterotypic interactions tend to be relatively strong (many k_BT), we focus on discussing the results at a high binding strength between $A-B$ sticker pairs (i.e., $\lambda \gg 1$). Furthermore, we consider

only the heterogeneous bonding limit, in which the stickers of A can only pair with those of B. It is straightforward to generalize the model described above to account for both self- and hetero-complementary linkages (i.e., $A-A$, $B-B$, and $A-B$.)

Results and Discussion

In this framework, we can show that reversible associations between A and B stickers compatibilize the polymer mixture by reducing the effective chemical incompatibility (lowering the "effective" χ_{AB} parameter) and driving a competition between associative and segregative phase separation. Associative phase separation into a sticker-poor phase in coexistence with a dense, highly associated network is favored at strong binding and low chemical incompatibility; while, segregative phase separation into A and B-rich phases is favored at weak binding and high chemical incompatibility. For both large degrees of chemical mismatch and strong binding conditions, the balance of attraction and repulsion results in microphase formation and eutectic-like behavior of the polymer alloy. Understanding the interplay of the chemical equilibrium of reversible binding and the tendency for phase separation will enable the development of a wide range of materials and applications. As such, we map out the phase diagrams, gelation conditions, and structures accessible to a solution or melt blend of multifunctional associative polymers that can be driven by molecular design, blend composition, binding interactions, or temperature.

Competition between Segregation and Sticker Binding

We first consider the competition between repulsions due to chemical incompatibility and attractions due to sticker binding by plotting the phase diagram as a function of the Flory–Huggins interaction parameter χ_{AB} and the association strength λ for a specific isopleth (line of constant composition). Figure 3 shows the gelation and phase coexistence conditions of heterotypic associating A and B chains at concentrations corresponding to a

binary melt with an overall composition $\phi_A = \phi_B = 0.5$. In our analysis, these phase boundaries will be referred to as lines of critical points (where the spinodal and binodal curves coincide).

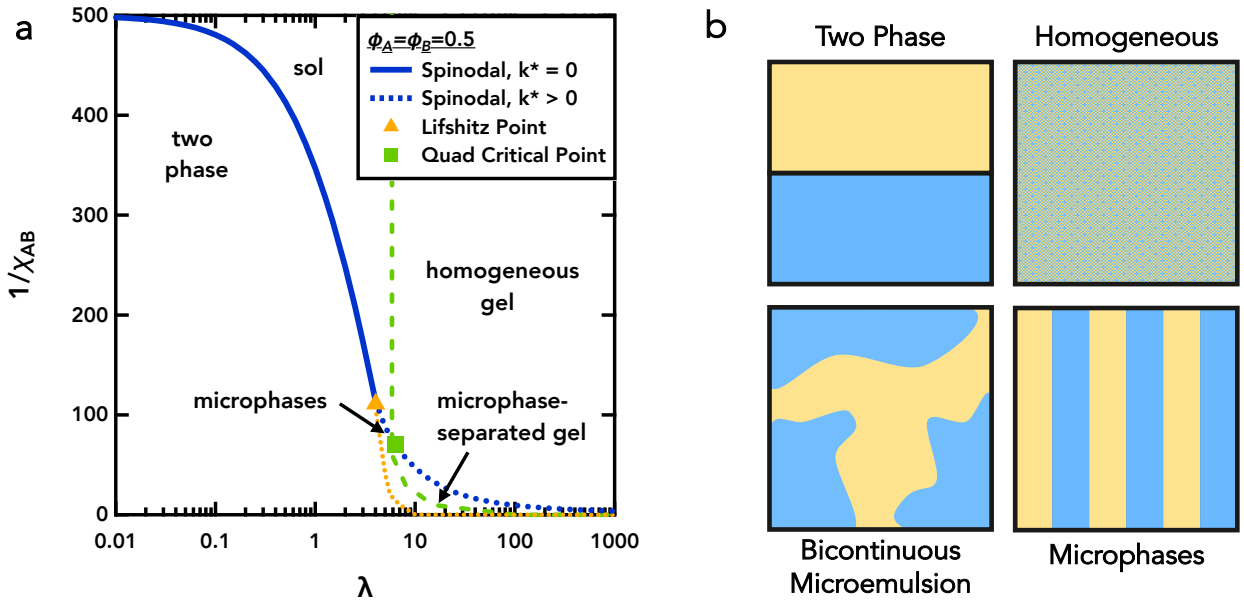

Figure 3: (a) Gelation (dashed green line) and phase coexistence conditions (blue lines) for associating polymers of type $A-B$ with $f_A = f_B = 20$ stickers, $s_A = s_B = 50$ spacers, $N_A = N_B = 1000$ degrees of polymerization, and $\phi_A = \phi_B = 0.5$. The solid blue line indicates spinodal decomposition at $k^* = 0$ (macrophase separation) and the dotted blue line indicates spinodal decomposition at $k^* > 0$ (microphase separation). The transition between macrophase and microphase separation is delineated by the dotted orange curve, which culminates at an isotropic Lifshitz point (coexistence between micro- and macrophase separation and the homogeneous one-phase) marked by an orange triangle. The gelation transition is delineated by the dashed green line passing through the quad-critical point (coexistence between sol, gel, microphases, and microphase-separated gel) as marked by a green square. (b) Schematic illustrations of the mixture in different phases.

Low Binding: Blend Compatibilization

Considering the phase behavior as λ tends to zero, there are few paired stickers, and the boundary between a homogeneous one-phase and macroscopic phase separation is delineated by a line of critical points with $k^* = 0$ (Figure 3). At these low binding conditions, above a critical segregation strength, the polymer mixture phase separates macroscopically into A-

and B-rich phases. Owing to osmotic compressibility and identical interaction parameters ($v_A = v_B$ and $w_A = w_B$), both phases have the same correlation length and overall concentration, differing only in the composition of A relative to B. The upper critical consolute point, the critical point at which raising χ_{AB} transforms a consolute liquid (fully miscible in all compositions) into a phase-separated mixture, is at $\chi_{AB} > 2/N$ for $N_A = N_B = N$ and $\phi_A = \phi_B = 1/2$ in the non-binding limit.[88–91]

As the bond association strength λ increases, the number of paired stickers grows, resulting in reversibly branched block copolymers. Thus, this line of critical points is related to the Scott line, which delineates the boundary between a disordered single-phase and macroscopic phase separation into A and B-rich phases, in A homopolymer, B homopolymer, AB block copolymer mixtures.[92,93] However, importantly, in the present case, the reversibility of the heterobonding has the consequence that the structure and connectivity are annealed. For low fraction of bonds, below the overlap of attractive volumes, as $\lambda \to 0$,

$$p_A \simeq \lambda \phi_B / s_B \ll 1 \tag{29}$$

and the terms in the free energy (eq. 11) related to associations take the form of pairwise attraction between stickers $-\lambda \phi_A \phi_B / (s_A s_B)$, reducing the χ_{AB} parameter for $A - B$ two-body interactions by the attractive volume fraction per monomer, $\lambda/(s_A s_B)$.[47] In this regime, corresponding to low conversion of stickers, the phase behavior can be described with the classical Flory–Huggins result for polymer blends[88–90] (or solutions in a non-selective solvent[91,94]) by replacing χ_{AB} by

$$\chi_{AB}^{\text{eff}} = \chi_{AB} - \lambda/(s_A s_B). \tag{30}$$

This implies that the physical associations between different species improve their miscibility. Accordingly, the boundary for phase separation shifts to higher χ_{AB} as the strength of sticker associations increases, i.e., compatibilization (shift to lower $1/\chi_{AB}$ in Figure 3).

It is the underlying reason why a phenomenological negative interaction parameter ($\chi_{AB} < 0$) is often successful at describing the interaction for associating polymers.[95,96] For example, blends of polystyrene/poly(xylenyl ether) (PS/PXE) are miscible in all proportions over a wide range of temperatures and molecular weights due to specific interactions between the PS phenyl rings and the PXE backbone; their phase behavior can be well described by simple solution theories using an effective interaction parameter of the form $\chi_{\mathrm{AB}} \sim -A + BT$ accounting for negative heat of mixing and negative local entropy of mixing.[97] Other miscible mixtures, including polyolefins, polycarbonates, and polyacrylates, have also been shown to require specific interactions between blend components to explain the temperature dependence of the measured negative interaction parameter.[98–102]

Such an approach essentially "smears" out the attractive sticker interactions over all monomers as an effective interaction parameter. It works in the limit of low degree of sticker conversion, below the overlap of attractive volumes, in which the fractional conversion increases linearly with the attractive volume fraction of stickers (eq. 29) and, accordingly, is valid for low association strengths,

$$\lambda < \left[\frac{\phi_A}{s_A} + \frac{\phi_B}{s_B}\right]^{-1}. \tag{31}$$

Thus, describing the system by an effective interaction parameter is ideal for homogeneous distributions of stickers with weak associations, as observed experimentally,[97–102] or with a smaller number of stickers that are more strongly associating, but spaced farther apart. This reinforces the balance of the excluded volume and chi interactions that occur between all monomers and the associative interactions that occur only between stickers.

Intermediate Binding: Micro-Ordering

With increasing λ, an increasing number of branched block copolymers form, becoming the dominant species. At this point, for a stoichiometric mixture of chains and stickers, there is

on average one bond per chain. The chemically dissimilar segments are now joined at the reticulation site of paired stickers and can only segregate locally rather than macroscopically, resulting in the appearance of microphases. This is a special tri-critical point in the phase diagram (Figure 3), called the Lifshitz point, which corresponds to the coexistence of macrophase separation (into A and B-rich phases), microphase separation (into a locally segregated ordered mesophase), and a disordered phase.[103]

At the mean-field level, the appearance of Lifshitz points does not significantly affect the phase diagram (Figure 3). However, outside the theory described in Section 2, Lifshitz points are known to be unstable to strong thermal fluctuations in three dimensions and are replaced by a narrow region of bicontinuous microemulsions, a highly structured sponge-like disordered phase.[16,104,105] Thus, it could be expected that the A and B-rich regions would contain solvent (if present) and unreacted homopolymers, but that more highly connected chains would be driven to the interface, resulting in essentially zero interfacial tension. Bicontinuous microemulsions are particularly important and interesting with regard to polymer alloys because the properties (e.g., permeability or conductivity) of one blend component are passed on to the entire material and the mechanical properties are maximized.[11,105] The use of multifunctional associating polymers to access this phase and tune their formation conditions should be advantageous.

Although the quantitative prediction of the location of the Lifshitz point depends on our approximation of the structural correlations as an effective 4-arm star copolymer (Figure 2), we expect that this would not be appreciably altered (by a factor of order unity) by a more complete description of the chain structures. Unlike most discussed Lifshitz points in polymer blends, where a single AB block copolymer species is added to a mixture of A and B homopolymers,[104,106,107] at our Lifshitz point, there is an ensemble of unreacted homopolymers with a statistical distribution of branched copolymers with two or more blocks/branches of various sizes and topologies. It would be interesting to check (experimentally with scattering or microscopy and computationally) if the inclusion of the higher order branched block

copolymers affects the structure of the bicontinuous microemulsions, perhaps by stabilizing select interfacial curvatures.[85,108–112]

Beyond the isotropic Lifshitz point, at a higher λ and thus more connected copolymers (with > 1 paired stickers per chain on average), there exists a line of critical points ($k^* \neq 0$) that correspond to the transition from a disordered phase to an ordered microphase with increasing χ_{AB} (Figure 3). This is often termed the Leibler line and occurs at $\chi_{AB}(N_A + N_B) \simeq 10.495$ for diblock copolymers or A_2B_2 4-arm star copolymers in mean-field theory.[113–115] However, in the present case, we have a mixture of differently bonded and branched copolymers (treated to first approximation as a mixture of non-bonded homopolymers and effective star block copolymers, Figure 2), with strand lengths that shorten with increased binding, $n_i = s_i/p_i$.

We have seen that small degrees of cross-linking can hinder macroscopic phase separation and induce microphases. On the contrary, it is well known that microphase separation is suppressed by increasing the cross-linking density.[7,85,116] The λ-dependent strand length is the primary reason for the increase in critical χ_{AB} needed for microphase separation. For macrophase separation of a binary blend of polymers A and B with degrees of polymerization $N_A = N_B$, the relevant parameter is $\chi_{AB}N_A = \chi_{AB}N_B$. For chains of A singly paired with chains of B, the relevant parameter for microphase separation is now $\chi_{AB}(N_A + N_B)$. As sticker binding increases and the lengths of the strands between the cross-links decrease, the relevant parameter for phase segregation also changes: $\chi_{AB}(n_A + n_B)$. At complete binding, this becomes $\chi_{AB}(s_A + s_B)$, which corresponds to the balance of entropy and chemical incompatibility of the strands. As the number of segments joined by a single cross-link decreases from $N_A + N_B$ to $s_A + s_B$ (as λ increases and more stickers are paired), the critical χ_{AB} necessary for microphase segregation also increases.

At a slightly higher λ, with a higher fraction of bonds, there are, on average, two paired stickers per chain, signaling the onset of gelation (eq. 7). The result is the appearance of what has been termed a quad-critical point, in which a single-phase (sol), microphase-

separated sol, homogeneous gel, and microphase-separated gel coexist. This quad-critical point is more aptly described as the gel point, as nothing special happens at the gelation threshold, since it is not thermodynamic, but rather a connectivity transition.[86] Below the gel point, the chains have yet to connect through the entire sample, but the elastic restoring forces between cross-linked A and B chains are still present, resulting in only local phase segregation: microphase separation takes place for λ both above and below the critical λ^{gel} for percolation (Figure 3). As we will see from the structural analysis of the microphases, the domain spacing $D^* = 2\pi/k^*$ is continuous at the gel point, diverging only at the Lifshitz point (when the mixture transitions between microphase and macrophase separation). This is in contrast to the connectivity length (i.e., the mesh size of the gel) which diverges at the gel point.[90]

In this analysis, we find that the Lifshitz point and the quad-critical point (gel point) are remarkably close (less than a factor of 2) in phase space in both χ_{AB} and λ (Figure 3). This agrees with previous work on end-linked miktoarm stars, wherein the points converge with increasing functionality of stickers from two to five,[30] and in the present analysis we have a 10× increase in the number of stickers per chain. Recall that the Lifshitz point corresponds to, on average, one cross-link per chain, and the gel point corresponds to, on average, two cross-links per chain. An interesting opportunity, with the gel point so close to the Lifshitz point, is the possibility for reversibly-"gelled" bicontinuous microemulsions, from which many applications could be envisaged.

High Binding: Connected Networks

For strong binding conditions, well above the overlap of attractive volumes, as $\lambda \to \infty$, the tendency is to form highly connected copolymer networks, again emphasizing the robust compatibilization effect of cross-linking the polymer blend. At high segregation strengths, these tight gels are primarily microphase separated, the structure of which is discussed below. However, the microphase and gelation boundaries tend towards higher values of λ

at higher χ_{AB}. It has been suggested that this occurs because the coexisting homogeneous phases become purer, limiting the ability to associate and form a network.[30,75] In our current framework, at the highest association and segregation strengths, we predict macroscopic phase separation into two coexisting gel phases and ultimately into two coexisting sol phases as χ_{AB} is increased. It is also possible that more "pure" microphases connected by sticker bonds localized to sharp interfaces are favored (relative to macrophase separation); however, the current weak inhomogeneity expansion-based theory does not account for chain stretching or sharp interfaces.

The conditions for these thermodynamic and connectivity transitions can be estimated by calculating an effective interaction parameter that describes attractive sticker interactions. In the limit of low sticker binding, as $\lambda \to 0$, we showed that these attractions could be described by the attractive volume per monomer $-\lambda/(s_A s_B)$ (eq. 30). A repulsive chi parameter of the same magnitude is required to overcome the sticker pairing. Across the entire range of bonding strengths, the sticker associations that balance the chemical incompatibility, at the stability limit of the mixture, takes the form:

$$\chi_{AB} \simeq \frac{p_A}{\phi_B s_A (1+\sqrt{r}p_A)} \simeq \frac{r p_A}{\phi_A s_B (1+\sqrt{r}p_A)} \tag{32}$$

This simple equality is obtained from the spinodal condition at $k = 0$ (in the $v = 0$, $w = 1$, and $N \to \infty$ limits). For strong binding strengths and strong segregation, where the physical behavior of the system is dominated by sticker attractions and chemical incompatibility, this should be a decent approximation of the phase boundary between homogeneous and microphase-segregated networks.

Considering $\lambda \gg 1$ (and $r = 1$) such that the stickers have gone to complete conversion ($p_A, p_B \to 1$), this balance of chemical incompatibility and sticker attraction becomes $\chi_{AB} \simeq 1/(\phi_B s_A) \simeq 1/(\phi_A s_B)$. For sticker stoichiometric mixtures, $r = 1$, we can further express

this condition as,

$$\chi_{AB} \simeq \frac{1}{s_A s_B}\sqrt{\frac{s_A}{\phi_A}}\sqrt{\frac{s_B}{\phi_B}} \tag{33}$$

which is inversely proportional to the geometric average sticker concentration $\sqrt{(\phi_A/s_A)(\phi_B/s_B)}$ normalized by the numbers of chemically dissimilar segments per strand s_A and s_B. For segregation strengths larger than eq. 33, the chemical incompatibility between A and B segments will start to break the reversible sticker bonds and drive macrophase separation.

For even stronger segregation, the degrees of conversion of A and B will continue to decrease. Eventually, at sufficiently large χ_{AB}, the chemical incompatibility will have driven enough bonds to break for the sample to de-percolate and transition from a gel to a sol. This condition can be estimated by considering eq. 33 as the amount of chemical incompatibility needed to break one sticker bond on average. Accordingly, to break $\sqrt{(f_A-1)(f_B-1)}$ cross-links to de-percolate the reversible network, segregation strengths larger than

$$\chi_{AB} \simeq \frac{\sqrt{(f_A-1)(f_B-1)}}{s_A s_B}\sqrt{\frac{s_A}{\phi_A}}\sqrt{\frac{s_B}{\phi_B}} \simeq \frac{1}{s_A s_B}\sqrt{\frac{N_A}{\phi_A}}\sqrt{\frac{N_B}{\phi_B}} \tag{34}$$

are needed (where in the second equality we have assumed $f_A, f_B \gg 1$.) The transition from microphase to macrophase separation of the strongly segregated gels is expected to occur on the same order of χ_{AB}, but intermediate to the conditions of eqs. 33-34. Full spatial calculations are likely required for accurate characterization of the microphases and phase boundary determination in such strongly segregated inhomogeneous gels.

Compositional Dependence

Next, we consider the effect of the Flory–Huggins interaction parameter χ_{AB} on the phase diagram of heterotypic associating A and B chains in a common, Θ solvent as a function of monomeric concentrations ϕ_A and ϕ_B (Figure 4). Although the system is a ternary incompressible mixture (A-polymer–B-polymer–solvent), it is convenient to examine the

dependence of the concentration ϕ_A relative to ϕ_B, with the solvent concentration $(1 - \phi_A - \phi_B)$ implicit. Note that in Figure 3, the phase boundaries shown are lines of critical points corresponding to both spinodal and binodal conditions. However, we should note that beyond the onset of eutectic behavior (discussed below), as $\lambda \to \infty$ and $1/(\chi_{AB}N) \to 0$, the isopleth spinodal may no longer be identical to the binodal condition, and should be considered approximate in Figure 3. In Figure 4, the spinodal (unstable) conditions for phase coexistence are shown.

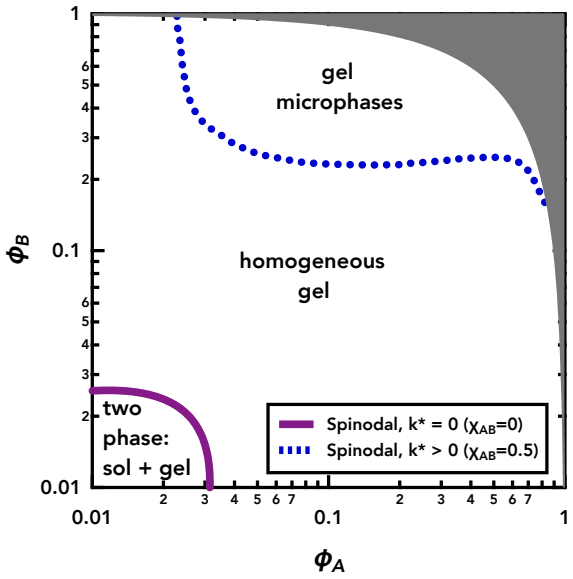

Figure 4: Phase diagram of a Θ-solution of $A - B$ associating polymers with $f_A = 20$, $f_B = 50$, $s_A = 50$, $s_B = 20$, $N_A = N_B = 10^4$, $v = 0$, $w = 1$, $\lambda = 500$, and $\chi_{AB} = 0.5$. The spinodal boundary for microphase separation is shown with a dotted blue line. The purple line shows the (macrophase) spinodal phase boundary in the absence of chemical incompatibility, $\chi_{AB} = 0$, for comparison. The shaded grey region is inaccessible due to incompressibility.

In the absence of chemical incompatibility ($\chi_{AB} = 0$, Figure 4), there is a two-phase region at low to intermediate monomeric concentrations. This macroscopic phase separation is caused by the associations between stickers, resulting in a dilute supernatant coexisting with a dense, more symmetric gel phase.[47] Note that the dilute coexisting phase is outside the applicability of and cannot be described by the current mean-field model, but it is expected that the concentration of this phase will be exponentially low. As the chemical incompatibil-

ity between the A and B chains increases, this region of associative phase separation shrinks and ultimately disappears at higher χ_{AB} (as shown for $\chi_{AB} = 0.5$ in Figure 4).

We can understand this trade-off between repulsive chemical incompatibility interactions and attractive sticker pairing by using the effective chi parameter from eq. 32. Increasing the bare chi parameter between A and B chains transforms the interactions from dominantly attractive to balanced (and thus, overall stable) to dominantly repulsive. Balanced net interactions occur at $\chi_{AB} \simeq p_A/[\phi_B s_A(1+\sqrt{r}p_A)]$ (eq. 32). At and above this condition, the effective repulsion between unlike segments (in the presence of an implicit solvent) stabilizes the polymer mixture at relatively low monomeric concentrations near the polymer overlap concentration $\phi^* = (\phi_A + \phi_B)^*$. This occurs by resisting condensation into a dense gel phase in which there is more $A-B$ repulsion induced by chemical incompatibility.

However, at higher total concentrations (concentrated solutions and melts), new regions of segregative phase separation appear in previously stable compositions[47] with increased chemical incompatibility, driven by the repulsion of dissimilar segments (Figure 4). A standard result of the Flory–Huggins model for chemically different polymers (without associations between stickers, $\lambda \to 0$) is that phase separation may occur when the interaction parameter χ_{AB} is positive and greater than a certain critical value:[88–91]

$$\chi_{AB} \geq \frac{1}{2}\left[\frac{1}{\phi_A N_A} + \frac{1}{\phi_B N_B}\right] \tag{35}$$

In contrast, for hetero-binding associative polymers, there is an absence of segregative phase separation at symmetric sticker conditions (Figure 4) that can be interpreted as compatibilization of the immiscible blend mixture. As in permanently cross-linked blends, the cross-linked system is more miscible than the non-cross-linked mixture.[7,117] The sticker attractions counteract the χ_{AB} repulsions driving phase separation. The result is the stability of a dense gel network with many paired stickers. Recall the balance of χ_{AB} and the effective attraction imposed by stickers, eq. 32, which shows that in this regime, the sticker

attractions simply reduce the effective chi, stabilizing the solution. However, microphase formation appears for melts and concentrated solutions with slightly off-stoichiometric stickers for A and B (Figure 4). Unlike sticker-stoichiometric gels that tend to remain homogeneous, there is an excess of unpaired stickers and their corresponding spacer strands. In highly non-stoichiometric mixtures, the excess can be macroscopically expelled from the gel; however, for near-stoichiometric mixtures, the elastic forces resulting from the presence of cross-links resist the natural tendency for macroscopic phase separation.[7,85] This competition drives local microphase separation, with the appearance of microdomains alternatively rich in A and B. The microphase separation regions flank the gel region in one phase at near-stoichiometric ratios of A to B stickers, indicating that for slight differences in the number of stickers, local segregation is advantageous.

Note that the gel condition (at lower concentrations than shown in Figure 4) is unchanged in our analysis by the increase in chemical incompatibility, as we do not account for the reduced contact and interpenetration of chains as a function of chemical incompatibility.[118–120] In part, this is due to our RPA framework, in which the concentrations are only weakly spatially varying, which is most appropriate for weak segregation strengths. Furthermore, we do not account for the spatial variation of the solvent, which has been shown to be enriched at $A-B$ interfaces, reducing the repulsion between A and B-rich domains.[121] Additionally, we have considered the case where the suspending solvent is not selective to either component of the blend. If the solvent preferentially solvates one species, it becomes consequential to account for micellar structures of the copolymers, reduction of chain interpenetration, and microdomain swelling to accurately describe the phase equilibria.[91,122,123]

For illustration, in Figure 4, we show the phase diagram for a mixture of chains with asymmetric numbers of stickers per chain $f_A \neq f_B$. In the absence of chemical incompatibility, the associative phase separation region is symmetric with respect to the sticker number densities ϕ_A/s_A and ϕ_B/s_B, highlighting that the sticker–sticker attractions drive phase separation.[47] Here, the associative phase separation region is weakly asymmetric and tilted

towards lower ϕ_B, due to the higher density of stickers on B chains relative to A chains, $s_B < s_A$. In the non-binding limit, the regions of segregative phase separation depend on the chain sizes N_A and N_B as well as the polymer volume fractions ϕ_A and ϕ_B, underscoring the importance of the balance between chemical incompatibility and translational entropy. Here, the segregative phase-separation regions resulting from the χ_{AB} interactions are substantially asymmetric because of the relative difference in the number of stickers per chain that can compatibilize the segments of A and B.

Importantly, the χ_{AB} repulsions act between all unlike monomers but are countered by associations that occur only between sticky monomers. This asymmetry in sticker density per chain, i.e., the size of the spacer between associative groups, leads to the strongest effects on the phase diagram and resultant physical behavior, which is why we have highlighted its effects in Figures 4-5. Collectively, these effects of various asymmetries highlight the importance of sticker mismatch in determining the phase behavior and physical properties of heterotypic associative polymers.[47]

The chemical compatibilization at near-stoichiometric sticker conditions and the effects of sticker mismatch can be explored more fully by looking at the χ_{AB}-dependence of the phase boundaries at a specific total concentration and varying the ratio of A to B. Figure 5 depicts the phase boundary in the coordinates of a temperature-like axis $(\chi_{AB}N)^{-1}$ versus $\phi_A = 1 - \phi_B$ (varying ratio of A to B in the absence of solvent). The phase envelope denotes the spinodal condition for macro- and microphase separation, with a local minimum at sticker stoichiometry: $\phi_A/s_A = \phi_B/s_B$ $(r = 1)$. For illustration, Figure 5 is shown for A and B chains with different spacer lengths between stickers, $s_A \neq s_B$. This results in an inherent asymmetry in both the compositional and temperature-like axes. The local minimum (maximum in χ_{AB} required for phase separation) occurs at,

$$\phi_A = s_B/(s_A + s_B) \tag{36}$$

which is $\phi_A = 0.714$ for the conditions in Figure 5, and can be described as a "eutectic point." At the eutectic composition (eq. 36), all stickers can bond, and the potential sticker attractions are at their strongest. Miscibility is substantially reduced for compositions away from the eutectic point, as unreacted stickers of the excess reactant are expelled from an otherwise highly connected network.

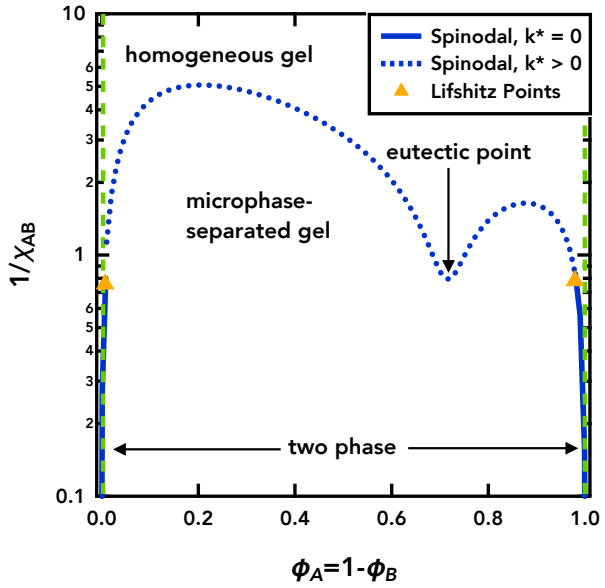

Figure 5: Gelation (dashed green lines) and spinodal conditions (solid and dotted blue lines) for associating polymers of type $A-B$ in a solvent-free blend $\phi_A + \phi_B = 1$ with $f_A = 20$, $f_B = 50$, $s_A = 50$, $s_B = 20$, $N = N_A = N_B = 1000$ at a fixed $\lambda = 10^4$ in the χ_{AB}^{-1}–ϕ_A plane. Lifshitz points are indicated by orange triangles.

The eutectic miscibility increases with λ, promoting the formation of a one-phase homogeneous gel at sticker stoichiometry. Raising χ_{AB} eventually induces phase separation in the eutectic composition at high enough segregation by breaking sticker bonds. Accordingly, we can use eq. 33, the chemical incompatibility necessary to break reversible bonds, to define a critical segregation strength at the eutectic point:

$$\chi_{AB}\left(\frac{s_A s_B}{s_A + s_B}\right) \simeq 10.5 \tag{37}$$

which is in decent agreement with the numerical result in Figure 5. Consequently, in a

metallurgical interpretation, we can define the two maxima in the spinodal in Figure 5 as "compounds." The approximate critical segregation strength at the compounds corresponds to the product $\chi_{AB}s_A$ for the compound at low ϕ_A and $\chi_{AB}s_B$ for the compound at low ϕ_B. These compounds should correspond to the compositions of the A and B-rich domains of the microphases. Within the microphase-separated region, altering the monomeric ratio of A to B, $\phi_A = 1-\phi_B$, simply alters the relative fraction of each domain within the microstructure, which would lead to different geometrical packing such as lamellae, cylinders, and spheres. The structure factors and domain spacing of these microphase-separated gels will be discussed below.

Notably, for the melt blend conditions considered in Figure 5, most compositions result in microphase separation. Otherwise, phase separation proceeds macroscopically into coexisting A-and B-rich gels, except for high segregation strengths, in which phase separation results in nearly pure A-and B-rich sol phases. The points at which the spinodal transitions from macro- to microphase separation are isotropic Lifshitz points—tri-critical points where homogeneous two-phase, homogeneous disordered, and microphase-separated regions coexist. The Lifshitz compositions occur at $\phi_A = 1 - \phi_B = 1/2(1 - N_A/(N_A + s_B) = 0.01$ and $\phi_A = 1/2(1 + N_B/(N_B + s_A)) = 0.98$. The Lifshitz compositions tend towards nearly pure A and B phases as the chain lengths N_A and N_B increase or the spacer lengths s_A and s_B decrease. Although our mean-field calculations do not capture the importance of fluctuations, it is known that Lifshitz compositions are accurately predicted by mean-field theory, at least for well-defined mixtures of homopolymers and diblock copolymers.[16] However, this might not be necessarily true in the present theory, where we approximated the associating mixture as 4-arm star copolymers and un-reacted homopolymers, particularly since the Lifshitz compositions are close to the component overlap concentrations, and thus, the boundary for applicability of mean-field.

Microdomain Structure and Properties

So far, we have focused on predicting the existence of microphase separation for the described reversible networks rather than on a description of the resultant structure. Various microphases can exist depending on the total concentration of the mixture and the relative composition of the polymer blend (melt or solution in a non-selective solvent). Naïvely, we would expect that near symmetric polymer volume fractions, the microphase formed should be lamellar in nature, whereas hexagonal or spherical structures could prevail for compositionally asymmetric mixtures.[49,124] However, we expect that for the multicomponent copolymer networks considered, random elastic forces will likely destroy long-range order, as is known for permanent networks in which orientational order and more ordered microstructures could result from anisotropic deformation.[125,126] In reality, Monte Carlo simulations of reversible multicomponent networks have shown topologically disordered networks with network rearrangement occurring cooperatively on scales larger than the distance between cross-links.[127] Further, randomly end-linked reversible copolymer networks have been shown to exhibit a wide window of co-continuous disordered phases.[10]

Thus, in general, we believe that the microphase separation is primarily local, where small regions alternately become more concentrated in A or B. We do not achieve a complete description of the microphase structure or symmetries, which would require much more elaborate calculations.[113] Stabilizing ordered phases and calculating coexistence is difficult in part because of the large distribution of unreacted homopolymers and complex branched copolymers. Homopolymers swell the microdomains of the ordered phases, whereas complex block copolymers would prefer the interfaces between A-and B-rich regions. Moreover, the stability of ordered phases at intermediate values of λ is possibly an artifact of the mean-field assumption, and fluctuation effects would cause the system to be disordered.[67,128–130]

Figure 6a-b illustrate the effects of λ and χ_{AB} on the structure factor of the associating polymer mixture. $S(k)$ has a maximum at the most probable concentration fluctuations $k^* \neq 0$. The peak narrows and grows in intensity with increasing χ_{AB} (Figure 6a), and

smears to a broad maximum at smaller distances (larger k) with increasing λ.[131] The scattering function diverges at the spinodal where the homogeneous melt is unstable to concentration fluctuations of wavelength $2\pi/k^*$, resulting in a microphase-separated structure with a domain size of $D^* = 2\pi/k^*$. Except for the macrophase-separating samples, in which $S(k)$ diverges at $k = 0$, the structure factor tends to zero because of the absence of quenched disorder, which is a consequence of the reversible nature of the cross-links. This conveniently allows us to avoid the need for replica methods necessary in permanent networks.[43] The broad tail of the structure factor is indicative of networks with correlations between sticker pairs at length scales smaller than the interfacial width of the domains.[126]

At a specified segregation strength $\chi_{AB} = 0.01$, the peak in $S(k)$ shifts to a smaller k as the strength of the sticker associations decreases from $\lambda = 100$ to 5, before ultimately diverging at $k = 0$ for low λ (Figure 6a), that is, macrophase separation in the limit of no sticker binding. Ignoring stretching due to strong segregation, at high λ, the domain size is minimized on the order of the Gaussian size of the spacers, $D^* \simeq a(s_A + s_B)^{1/2}$. Upon decreasing sticker association strength, the domain periodicity of the microphase separation increases steadily as the average number of segments in the strand between the reticulation points, s_A/p_A and s_B/p_B, increases (Figure 6c,e). Notably, this implies that the domain size can be approximated as the Gaussian size of the copolymer strands around the cross-link (recall "effective" star polymer, Figure 2):

$$D^* \simeq a\left(\frac{s_A}{p_A} + \frac{s_B}{p_B}\right)^{1/2} \tag{38}$$

until finally diverging at the Lifshitz point. At low λ, the polymers macrophase separate; at slightly higher λ, the polymers microphase separate with a domain spacing of the order of the Gaussian size (R_0) of a singly cross-linked A and B 4-arm ($f = 4$) star:[132] $D^* \simeq R_0 \simeq af^{1/4}((N_A + N_B)/4)^{1/2}$ (Figure 6c). Note that nothing special occurs with the domain spacing at the gelation threshold. At high association, the domain periodicity tends towards

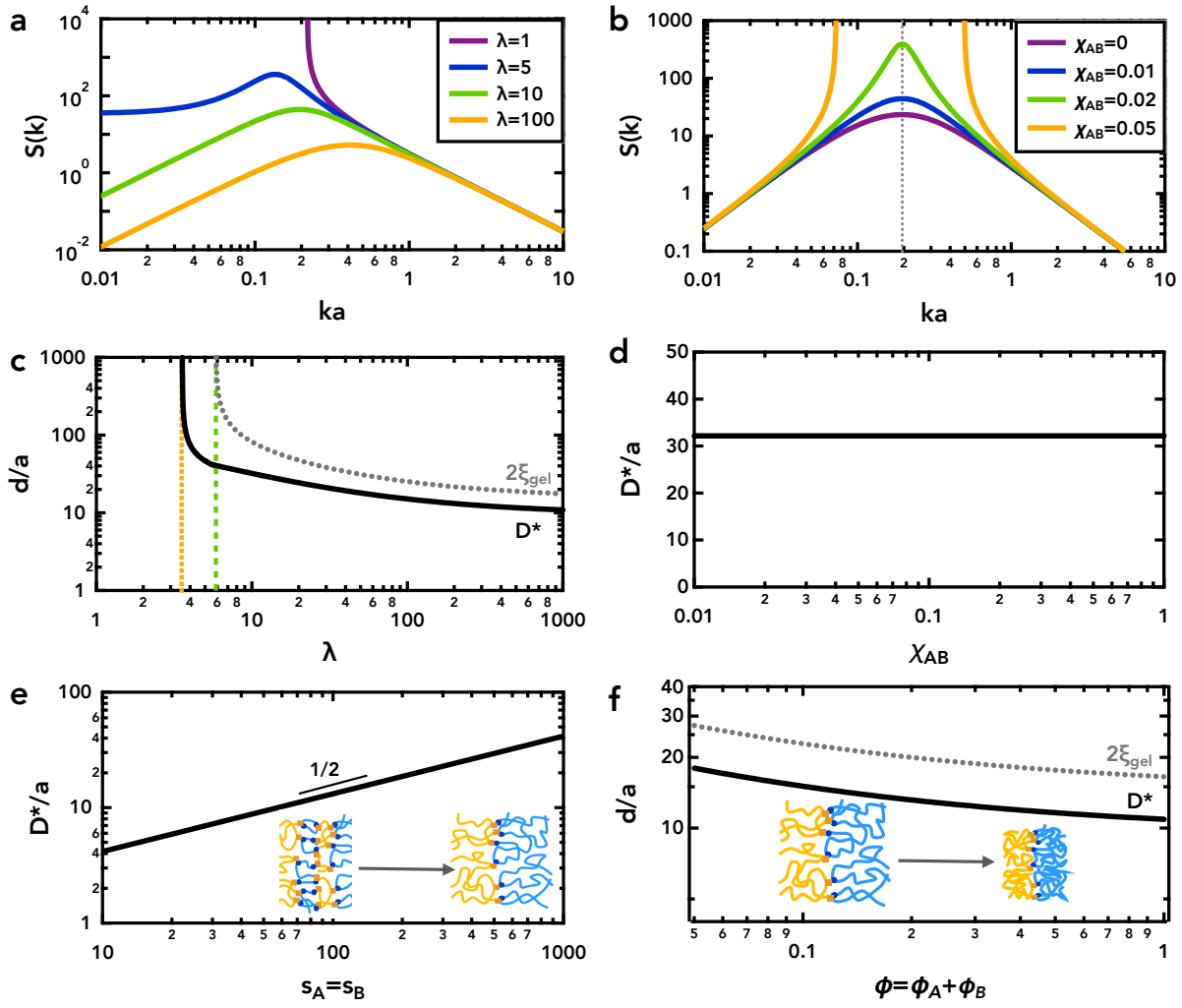

Figure 6: (a,b) Structure factor and (c-f) characteristic length-scales for $A-B$ associating polymers with $\phi_A = \phi_B = 0.5$, $f_A = f_B = 20$, $s_A = s_B = 50$, $N_A = N_B = 1000$, $v = 0$, and $w = 1$ (unless otherwise noted) for different bonding strengths and chemical incompatibility. (a) The structure factor weakens and shifts to higher k for fixed $\chi_{AB} = 0.01$ with increasing λ. (b) The structure factor intensifies for fixed $\lambda = 10$ with increasing χ_{AB}. (c) The domain size at fixed $\chi_{AB} = 0.01$ is strongly dependent on λ. The dashed green line indicates the gel point, and the dotted orange line indicates the Lifshitz point and a divergence in the domain size. The mesh size of the gel ξ_{gel}, the connectivity length scale, diverges at the gel point. (d) The domain size for fixed $\lambda = 10$ is independent of the chemical incompatibility. (e) The domain size increases as the square root of the number of segments in the spacer. $N_A = N_B = 10^5$, $\lambda = 1000$, $\chi_{AB} = 0.1$ (f) The domain size and mesh size of the gel decrease with increasing polymer volume fraction. $N_A = N_B = 10^5$, $\lambda = 1000$, $\chi_{AB} = 0.1$.

twice the mesh size of the network, i.e., the distance between cross-links, approximated as

$$\xi_{\text{gel}} = R_0 \left(\frac{p_A}{p_A^{\text{gel}}} - 1 \right)^{-1/2} \left(\frac{p_B}{p_B^{\text{gel}}} - 1 \right)^{-1/2} \tag{39}$$

However, this connectivity length diverges at the gel point as the network loses percolation, while the domain spacing remains a continuous function of λ (Figure 6c). This is because the paired stickers have yet to percolate, but still drive a critical length scale for the copolymer to locally phase segregate.

In contrast, for a specified sticker association strength $\lambda = 10$, the peak in $S(k)$ intensifies at the same wave number, and the domain size is seemingly unperturbed by an increase in the segregation strength (Figure 6b,d). While this is in good agreement with the theory and simulations of permanently cross-linked polymer blends[7,86,127,131] it is contrary to simulations of reversibly associating blends[31] and might be an artifact of our RPA approach, which is most appropriate for weak segregation. Because the cross-links are reversible, we might otherwise expect the microdomains to be better described by strong segregation theory (as for block copolymers), in which we would expect stretched domains of size $D^* \simeq an^{2/3}\chi_{AB}^{1/6}$, where n is the strand length.[133,134] Additionally, direct comparisons between linear diblock copolymers and star copolymers (such as the A_2B_2 "effective" network strand we consider, Figure 2), have shown that the entropic penalty of junction points localized to the $A-B$ interface increases chain stretching and domain elongation.[135,136] The present theory could be expanded to account for such effects.

The period of the microdomains is also a decreasing function of the concentration, owing to the reduced sticker association (Figure 6f). Recall that chain stretching due to swelling or strong segregation was not included in the current model. The scaling of the domain size with the total polymer volume fraction follows the same dependence as the gel connectivity over these conditions (away from the gel point). Thus, we can conclude that the microphase separation is dominated by the topological properties of the network, at least for weak

segregation (relative to sticker association). This can be justified by the expectation that the $A-B$ cross-links are localized at the interface between the A and B-rich domains, and that the gel connectivity dictates the accessible length scale for phase segregation. This is in agreement with recent simulations by the Jayaraman group, which demonstrated the importance of sticker placement along the chain on the resultant microdomains.[31] These results give additional handles on the molecular design of these materials, as the domain size can be adjusted by changing the size of the spacers between sticky groups or by the concentration of the mixture (Figure 6e,f).

Conclusions

The physical system we have considered is a mixture of two multifunctional hetero-associating polymers A and B of different chemical nature. The aim was to study the effects of chemical incompatibility on the reversible network formation and corresponding phase behavior using an extension of the mean-field model for $A-B$ associative polymers to account for local compositional fluctuations. Using this model, we calculated the structure factor, which allowed us to determine the microphase properties.

The central result is that reversible bonds between hetero-complementary associating groups can compatibilize immiscible polymer blends. The transient cross-links formed by the associations form branched block copolymers, which can percolate the system to create copolymer networks. These networks, both dry elastomers and gels swollen with a solvent, exhibit eutectic-like behavior. At higher degrees of chemical incompatibility, the networks assemble into microphase-separated domains because the elasticity imparted by the cross-links resists macroscopic phase separation, establishing a microscopic domain size. The resultant microdomain structure can be tuned by adjusting the association and segregation strengths, concentration, and spacer size between stickers.

These results are the first comprehensive theoretical description of the chemical compat-

ibilization and macro- and microphase separation of mixtures of associating polymers with numerous stickers per chain. In the limit of low chemical incompatibility, the model reduces to prior mean-field models of associative polymers.[47] At strong binding conditions ($\lambda \to \infty$), the results are consistent with scaling model, random phase approximation, and molecular dynamics simulations predictions of permanently cross-linked polymer blends.[7,84,86,131,137–139] Furthermore, the results are qualitatively consistent with field-theoretic simulation predictions for reversibly end-linked tri- and tetra-functional associative polymers[30,140] and coarse-grained molecular dynamics simulations of regularly spaced Hydrogen bonding blends.[31]

We can easily extend the formalism presented here to a mixed bonding case, where $A-A$, $A-B$, and $B-B$ cross-links all occur in the polymer mixture. In this case, hetero-bonding competes with homo-bonding, depending on the relative strength of the associations, i.e., $\epsilon_{AB} >$ or $< \epsilon_{AA}, \epsilon_{BB}$. As illustrated for the simple case of heterotypic $A-B$ associations, the presence of hetero-bonded chains (i.e., copolymers) can stabilize mesophases that compete with homogeneous phases.

For simplicity, we considered the equilibrium conditions; however, there is a complex interplay between the kinetics of gelation and phase separation.[117] In particular, we have described simultaneous associations and segregation, but the order of sample processing might dictate the resultant physical properties. For example, at high $\chi_{AB}N$, strongly segregated mixtures can affect the ability of unlike stickers to find each other and cross-link, thereby shifting the gelation conditions. Away from equilibrium, in loosely associated systems (with the distance between entanglements smaller than the distance between cross-links), the presence of trapped entanglements would act as cross-links[85,139] enhancing compatibilization and favoring microphase formation rather than macroscopic phase separation.

Although we have explored the gelation and phase behavior across a range of temperatures by varying both χ_{AB} and λ, we have attempted to focus on describing the limiting behaviors and identifying opportunities for further study. Accurately describing the transition from segregation-dominated to binding-dominated regimes will require more sophisticated

treatment and numerical implementation of the chain statistics of all branching (and looping) reaction products. One main advantage of the current methodology is that it allows one to re-create the salient physical description of blend compatibilization, reversible gelation, and microphase formation with a minimal model that can be computed analytically.

We are keenly interested in relating our theoretical work to experiments. Although previous work demonstrated compatibilization and the transition between macro- and microphase separation for supramolecular copolymers, we are unaware of any experiments that have systematically explored the phase diagrams and structures formed by multifunctional associating polymer blends. Prediction of gelation and phase behavior can be systematically tested by preparing mixtures of associating polymers at different concentrations. In particular, eutectic behavior should be easily verifiable for a melt blend of high χ_{AB} polymers with strongly associating hydrogen bonding or ionic groups sparsely distributed along the chains. The order–disorder transition temperature (ODT), as measured by X-ray scattering, is sticker-stoichiometry-dependent and is suppressed at matched sticker concentrations. While the entire range of binding and segregation conditions is likely not accessible within a single polymer blend, choosing systems with stickers of varied association strengths and different regions of phase space should be accessible for validation.

The physical properties of these copolymer networks are of high interest and importance,[43] in part, for their implications for biological condensates[39,40] and potential utility in polymer reprocessing.[141–144] For microphase-separated gels, control over domain size, by temperature, concentration, and polymer architecture enables optically and mechanically responsive materials. In particular, near the microphase and gelation transitions, optical transparency could be switchable as the domain sizes change relative to the wavelength of light.[145,146] For microphase formation in solution, rather than in melts, the final network will show porosity at small and adjustable length scales, which could be useful for templating separation membranes.[147,148] Ultimately, the mechanical properties of these networks will be highly controllable by the mesophase and network percolation, in addition to the

cross-link density and lifetimes. Furthermore, for polymers with additional functionalities, such controllable connectivity and microphase formation could be utilized for confined enzymatic activity,[149] drug encapsulation,[150,151] or micro-structured conductive pathways.[152–154] Accordingly, our results are expected to be useful in the design and development of new reversibly bonded materials. Future work will seek to develop theoretical models to predict the mechanics and dynamics of associating polymer blends.

Acknowledgement

This work was supported by the NSF Center for the Chemistry of Molecularly Optimized Networks (MONET), CHE-2116298. The author thanks all the members of the MONET Center for insightful discussions, as well as Michael Rubinstein and Steve Craig for assistance in preparing the manuscript.

References

(1) Paul, D. R.; Newman, S. *Polymer Blends*; Academic Press: New York, 1978.

(2) Paul, D. R.; Vinson, C. E.; Locke, C. E. Potential for Reuse of Plastics Recovered from Solid Wastes. *Polym. Eng. Sci.* **1972**, *12*, 157–166, DOI: 10.1002/pen.760120302.

(3) Barlow, J. W.; Paul, D. R. Polymer Blends and Alloys - a Review of Selected Considerations. *Polym. Eng. Sci.* **1981**, *21*, 985–996, DOI: 10.1002/pen.760211502.

(4) Briber, R. M.; Bauer, B. J. Effect of Cross-Links on the Phase-Separation Behavior of a Miscible Polymer Blend. *Macromolecules* **1988**, *21*, 3296–3303, DOI: 10.1021/ma00189a026.

(5) Sakurai, S.; Iwane, K.; Nomura, S. Morphology of Poly(Styrene-block-Butadiene-block-Styrene) Triblock Copolymers Cross-Linked in the Disordered State. *Macromolecules* **1993**, *26*, 5479–5486, DOI: 10.1021/ma00072a028.

(6) Hahn, H.; Eitouni, H. B.; Balsara, N. P.; Pople, J. A. Responsive Solids from Cross-Linked Block Copolymers. *Phys. Rev. Lett.* **2003**, *90*, 155505, DOI: 10.1103/PhysRevLett.90.155505.

(7) de Gennes, P. G. Effect of Cross-Links on a Mixture of Polymers. *J. Phys., Lett.* **1979**, *40*, L69–L72.

(8) Asnaghi, D.; Giglio, M.; Bossi, A.; Righetti, P. G. Large-Scale Microsegregation in Polyacrylamide Gels (Spinodal Gels). *J. Chem. Phys.* **1995**, *102*, 9736–9742, DOI: 10.1063/1.468792.

(9) Panyukov, S.; Rabin, Y. Polymer Gels: Frozen Inhomogeneities and Density Fluctuations. *Macromolecules* **1996**, *29*, 7960–7975, DOI: 10.1021/ma960164t.

(10) Zeng, D.; Hayward, R. C. Effects of Randomly End-Linked Copolymer Network Parameters on the Formation of Disordered Cocontinuous Phases. *Macromolecules* **2019**, *52*, 2642–2650, DOI: 10.1021/acs.macromol.9b00050.

(11) Düchs, D.; Ganesan, V.; Fredrickson, G. H.; Schmid, F. Fluctuation Effects in Ternary AB+A+B Polymeric Emulsions. *Macromolecules* **2003**, *36*, 9237–9248, DOI: 10.1021/ma030201y.

(12) Anastasiadis, S. H.; Gancarz, I.; Koberstein, J. T. Compatibilizing Effect of Block Copolymers Added to the Polymer/Polymer Interface. *Macromolecules* **1989**, *22*, 1449–1453, DOI: 10.1021/ma00193a074.

(13) Dai, C. A.; Dair, B. J.; Dai, K. H.; Ober, C. K.; Kramer, E. J.; Hui, C. Y.; Jelinski, L. W. Reinforcement of Polymer Interfaces with Random Copolymers. *Phys. Rev. Lett.* **1994**, *73*, 2472–2475, DOI: 10.1103/PhysRevLett.73.2472.

(14) Macosko, C. W.; Guegan, P.; Khandpur, A. K.; Nakayama, A.; Marechal, P.; Inoue, T. Compatibilizers for Melt Blending: Premade Block Copolymers. *Macromolecules* **1996**, *29*, 5590–5598, DOI: 10.1021/ma9602482.

(15) Self, J. L.; Zervoudakis, A. J.; Peng, X. Y.; Lenart, W. R.; Macosko, C. W.; Ellison, C. J. Linear, Graft, and Beyond: Multiblock Copolymers as Next-Generation Compatibilizers. *JACS Au* **2022**, *2*, 310–321, DOI: 10.1021/jacsau.1c00500.

(16) Fredrickson, G. H.; Bates, F. S. Design of Bicontinuous Polymeric Microemulsions. *J. Polym. Sci. B: Polym. Phys.* **1997**, *35*, 2775–2786, DOI: 10.1002/(Sici)1099-0488(199712).

(17) Pernot, H.; Baumert, M.; Court, F.; Leibler, L. Design and Properties of Co-Continuous Nanostructured Polymers by Reactive Blending. *Nat. Mater.* **2002**, *1*, 54–58, DOI: 10.1038/nmat711.

(18) Macosko, C. W.; Jeon, H. K.; Hoye, T. R. Reactions at Polymer–Polymer Interfaces for Blend Compatibilization. *Prog. Polym. Sci.* **2005**, *30*, 939–947, DOI: 10.1016/j.progpolymsci.2005.06.003.

(19) Xanthos, M.; Dagli, S. S. Compatibilization of Polymer Blends by Reactive Processing. *Polym. Eng. Sci.* **1991**, *31*, 929–935, DOI: 10.1002/pen.760311302.

(20) Xie, S. Y.; Karnaukh, K. M.; Yang, K. C.; Sun, D.; Delaney, K. T.; de Alaniz, J. R.; Fredrickson, G. H.; Segalman, R. A. Compatibilization of Polymer Blends by Ionic Bonding. *Macromolecules* **2023**, *56*, 3617–3630, DOI: 10.1021/acs.macromol.3c00060.

(21) Huh, J.; Park, H. J.; Kim, K. H.; Kim, K. H.; Park, C.; Jo, W. H. Giant Thermal Tunability of the Lamellar Spacing in Block-Copolymer-Like Supramolecules Formed from Binary-End-Functionalized Polymer Blends. *Adv. Mater.* **2006**, *18*, 624–629, DOI: 10.1002/adma.200500963.

(22) Feldman, K. E.; Kade, M. J.; de Greef, T. F. A.; Meijer, E. W.; Kramer, E. J.; Hawker, C. J. Polymers with Multiple Hydrogen-Bonded End Groups and Their Blends. *Macromolecules* **2008**, *41*, 4694–4700, DOI: 10.1021/ma800375r.

(23) Feldman, K. E.; Kade, M. J.; Meijer, E. W.; Hawker, C. J.; Kramer, E. J. Phase Behavior of Complementary Multiply Hydrogen Bonded End-Functional Polymer Blends. *Macromolecules* **2010**, *43*, 5121–5127, DOI: 10.1021/ma1003776.

(24) Lin, Y. H.; Darling, S. B.; Nikiforov, M. O.; Strzalka, J.; Verduzco, R. Supramolecular Conjugated Block Copolymers. *Macromolecules* **2012**, *45*, 6571–6579, DOI: 10.1021/ma300829u.

(25) Rubinstein, M.; Dobrynin, A. V. Associations Leading to Formation of Reversible Networks and Gels. *Curr. Opin. Colloid Interface Sci.* **1999**, *4*, 83–87, DOI: 10.1016/S1359-0294(99)00013-8.

(26) Zhang, Z. J.; Chen, Q.; Colby, R. H. Dynamics of Associative Polymers. *Soft Matter* **2018**, *14*, 2961–2977, DOI: 10.1039/c8sm00044a.

(27) Wu, S. L.; Chen, Q. Advances and New Opportunities in the Rheology of Physically and Chemically Reversible Polymers. *Macromolecules* **2022**, *55*, 697–714, DOI: 10.1021/acs.macromol.1c01605.

(28) Fredrickson, G. H.; Xie, S. Y.; Edmund, J.; Le, M. L.; Sun, D.; Grzetic, D. J.; Vigil, D. L.; Delaney, K. T.; Chabinyc, M. L.; Segalman, R. A. Ionic Compatibilization of Polymers. *ACS Polymers Au* **2022**, *2*, 299–312, DOI: 10.1021/acspolymersau.2c00026.

(29) Tanaka, F.; Ishida, M. Microphase Formation in Mixtures of Associating Polymers. *Macromolecules* **1997**, *30*, 1836–1844, DOI: 10.1021/ma961457p.

(30) Mester, Z.; Mohan, A.; Fredrickson, G. H. Macro- and Microphase Separation in Multifunctional Supramolecular Polymer Networks. *Macromolecules* **2011**, *44*, 9411–9423, DOI: 10.1021/ma201551c.

(31) Kulshreshtha, A.; Hayward, R. C.; Jayaraman, A. Impact of Composition and Placement of Hydrogen-Bonding Groups along Polymer Chains on Blend Phase Behavior: Coarse-Grained Molecular Dynamics Simulation Study. *Macromolecules* **2022**, *55*, 2675–2690, DOI: 10.1021/acs.macromol.2c00055.

(32) Cordier, P.; Tournilhac, F.; Soulie-Ziakovic, C.; Leibler, L. Self-Healing and Thermoreversible Rubber from Supramolecular Assembly. *Nature* **2008**, *451*, 977–980, DOI: 10.1038/nature06669.

(33) Syrett, J. A.; Becer, C. R.; Haddleton, D. M. Self-Healing and Self-Mendable Polymers. *Polym. Chem.* **2010**, *1*, 978–987, DOI: 10.1039/c0py00104j.

(34) Wojtecki, R. J.; Meador, M. A.; Rowan, S. J. Using the Dynamic Bond to Access Macroscopically Responsive Structurally Dynamic Polymers. *Nat. Mater.* **2011**, *10*, 14–27, DOI: 10.1038/Nmat2891.

(35) Stukalin, E. B.; Cai, L. H.; Kumar, N. A.; Leibler, L.; Rubinstein, M. Self-Healing of Unentangled Polymer Networks with Reversible Bonds. *Macromolecules* **2013**, *46*, 7525–7541, DOI: 10.1021/ma401111n.

(36) Campanella, A.; Dohler, D.; Binder, W. H. Self-Healing in Supramolecular Polymers. *Macromol. Rapid Commun.* **2018**, *39*, 1700739, DOI: 10.1002/marc.201700739.

(37) Li, P. L.; Banjade, S.; Cheng, H. C.; Kim, S.; Chen, B.; Guo, L.; Llaguno, M.; Hollingsworth, J. V.; King, D. S.; Banani, S. F.; Russo, P. S.; Jiang, Q. X.; Nixon, B. T.; Rosen, M. K. Phase Transitions in the Assembly of Multivalent Signalling Proteins. *Nature* **2012**, *483*, 336–U129, DOI: 10.1038/nature10879.

(38) Feric, M.; Vaidya, N.; Harmon, T. S.; Mitrea, D. M.; Zhu, L.; Richardson, T. M.; Kriwacki, R. W.; Pappu, R. V.; Brangwynne, C. P. Coexisting Liquid Phases Underlie Nucleolar Subcompartments. *Cell* **2016**, *165*, 1686–1697, DOI: 10.1016/j.cell.2016.04.047.

(39) Boeynaems, S.; Holehouse, A. S.; Weinhardt, V.; Kovacs, D.; Van Lindt, J.; Larabell, C.; Van Den Bosch, L.; Das, R.; Tompa, P. S.; Pappu, R. V.; Gitler, A. D. Spontaneous Driving Forces Give Rise to Protein-RNA Condensates with Coexisting Phases and Complex Material Properties. *Proc. Natl. Acad. Sci. U.S.A.* **2019**, *116*, 7889–7898, DOI: 10.1073/pnas.1821038116.

(40) Hildebrand, E. M.; Dekker, J. Mechanisms and Functions of Chromosome Compartmentalization. *Trends Biochem. Sci.* **2020**, *45*, 385–396, DOI: 10.1016/j.tibs.2020.01.002.

(41) Brackley, C. A.; Marenduzzo, D. Bridging-Induced Microphase Separation: Photobleaching Experiments, Chromatin Domains and the Need for Active Reactions. *Brief. Funct. Genomics* **2020**, *19*, 111–118, DOI: 10.1093/bfgp/elz032.

(42) Hilbert, L.; Sato, Y.; Kuznetsova, K.; Bianucci, T.; Kimura, H.; Julicher, F.; Honigmann, A.; Zaburdaev, V.; Vastenhouw, N. L. Transcription Organizes Euchromatin via Microphase Separation. *Nat. Commun.* **2021**, *12*, 1360, DOI: 10.1038/s41467-021-21589-3.

(43) Danielsen, S. P. O.; Beech, H. K.; Wang, S.; El-Zaatari, B. M.; Wang, X.; Sapir, L.; Ouchi, T.; Wang, Z.; Johnson, P. N.; Hu, Y.; Lundberg, D. J.; Stoychev, G.; Craig, S. L.; Johnson, J. A.; Kalow, J. A.; Olsen, B. D.; Rubinstein, M. Molecular Characterization of Polymer Networks. *Chem. Rev.* **2021**, *121*, 5042–5092, DOI: 10.1021/acs.chemrev.0c01304.

(44) Painter, P. C.; Graf, J.; Coleman, M. M. A Lattice Model Describing Hydrogen-Bonding in Polymer Mixtures. *J. Chem. Phys.* **1990**, *92*, 6166–6174, DOI: 10.1063/1.458340.

(45) Semenov, A. N.; Joanny, J. F.; Khokhlov, A. R. Associating Polymers: Equilibrium and Linear Viscoelasticity. *Macromolecules* **1995**, *28*, 1066–1075, DOI: 10.1021/ma00108a038.

(46) Semenov, A. N.; Rubinstein, M. Thermoreversible Gelation in Solutions of Associative Polymers. 1. Statics. *Macromolecules* **1998**, *31*, 1373–1385, DOI: 10.1021/ma970616h.

(47) Danielsen, S. P. O.; Semenov, A. N.; Rubinstein, M. Phase Separation and Gelation in Solutions of Hetero-Associative Polymers. *ChemRxiv* **2023**, 1–58, DOI: 10.26434/chemrxiv-2023-1hz22.

(48) Angerman, H. J.; ten Brinke, G. Weak Segregation Theory of Microphase Separation

in Associating Binary Homopolymer Blends. *Macromolecules* **1999**, *32*, 6813–6820, DOI: 10.1021/ma981518e.

(49) Fredrickson, G. H.; Delaney, K. T. Coherent States Field Theory in Supramolecular Polymer Physics. *J. Chem. Phys.* **2018**, *148*, 204904, DOI: 10.1063/1.5027582.

(50) Hoy, R. S.; Fredrickson, G. H. Thermoreversible Associating Polymer Networks. I. Interplay of Thermodynamics, Chemical Kinetics, and Polymer Physics. *J. Chem. Phys.* **2009**, *131*, 224902, DOI: 10.1063/1.3268777.

(51) Tanaka, F.; Ishida, N. Thermoreversible Gelation with Two-Component Networks. *Macromolecules* **1999**, *32*, 1271–1283, DOI: 10.1021/ma981279v.

(52) Tanaka, F. Thermoreversible Gelation with Two-Component Mixed Cross-Link Junctions of Variable Multiplicity in Ternary Polymer Solutions. *Gels* **2021**, *7*, 89, DOI: 10.3390/gels7030089.

(53) Zhang, Y. J.; Xu, B.; Weiner, B. G.; Meir, Y.; Wingreen, N. S. Decoding the Physical Principles of Two-Component Biomolecular Phase Separation. *eLife* **2021**, *10*, e62403, DOI: 10.7554/eLife.62403.

(54) Choi, J. M.; Holehouse, A. S.; Pappu, R. V. Physical Principles Underlying the Complex Biology of Intracellular Phase Transitions. *Annu. Rev. Biophys.* **2020**, *49*, 107–133, DOI: 10.1146/annurev-biophys-121219-081629.

(55) Jayaraman, A. 100th Anniversary of Macromolecular Science Viewpoint: Modeling and Simulation of Macromolecules with Hydrogen Bonds: Challenges, Successes, and Opportunities. *ACS Macro Lett.* **2020**, *9*, 656–665, DOI: 10.1021/acsmacrolett.0c00134.

(56) Prusty, D.; Pryamitsyn, V.; de la Cruz, M. O. Thermodynamics of As-

sociative Polymer Blends. *Macromolecules* **2018**, *51*, 5918–5932, DOI: 10.1021/acs.macromol.8b00661.

(57) Kramarenko, E. Y.; Erukhimovich, I. Y.; Khokhlov, A. R. The Influence of Ion Pair Formation on the Phase Behavior of Polyelectrolyte Solutions. *Macromol. Theory Simul.* **2002**, *11*, 462–471, DOI: 10.1002/1521-3919(20020601)11:5<462::Aid-Mats462>3.0.Co;2-K.

(58) Rumyantsev, A. M.; Kramarenko, E. Y. Two Regions of Microphase Separation in Ion-Containing Polymer Solutions. *Soft Matter* **2017**, *13*, 6831–6844, DOI: 10.1039/c7sm01340j.

(59) Erel, I.; Zhu, Z. C.; Sukhishvili, S.; Patyukova, E.; Potemkin, I.; Kramarenko, E. Two Types of Block Copolymer Micelles with Ion-Containing Cores. *Macromol. Rapid Commun.* **2010**, *31*, 490–495, DOI: 10.1002/marc.200900659.

(60) Rumyantsev, A. M.; Kramarenko, E. Y. Effect of Ion Pair Formation on the Structure of Polymer Micelles with Ionic Amphiphilic Coronae. *J. Chem. Phys.* **2013**, *138*, 204904, DOI: 10.1063/1.4807005.

(61) Kudlay, A.; Ermoshkin, A. V.; de la Cruz, M. O. Complexation of Oppositely Charged Polyelectrolytes: Effect of Ion Pair Formation. *Macromolecules* **2004**, *37*, 9231–9241, DOI: 10.1021/ma048519t.

(62) Flory, P. J. Molecular size distribution in three dimensional polymers. I. Gelation. *J. Am. Chem. Soc.* **1941**, *63*, 3083–3090, DOI: 10.1021/ja01856a061.

(63) Stockmayer, W. H. Molecular Distribution in Condensation Polymers. *J. Polym. Sci.* **1952**, *9*, 69–71, DOI: 10.1002/pol.1952.120090106.

(64) Macosko, C. W.; Miller, D. R. New Derivation of Average Molecular-Weights of Nonlinear Polymers. *Macromolecules* **1976**, *9*, 199–206, DOI: 10.1021/ma60050a003.

(65) Miller, D. R.; Macosko, C. W. New Derivation of Post Gel Properties of Network Polymers. *Macromolecules* **1976**, *9*, 206–211, DOI: 10.1021/ma60050a004.

(66) Zaldivar, G.; Tagliazucchi, M. Layer-by-Layer Self-Assembly of Polymers with Pairing Interactions. *ACS Macro Lett.* **2016**, *5*, 862–866, DOI: 10.1021/acsmacrolett.6b00258.

(67) Fredrickson, G. H. *The Equilibrium Theory of Inhomogeneous Polymers*; Oxford University Press, 2006.

(68) de Gennes, P. G. *Scaling Concepts in Polymer Physics*; Cornell University Press: Ithaca, NY, 1979.

(69) Vilgis, T. A.; Benmouna, M.; Benoit, H. Static Scattering from Multicomponent Polymer Systems: Theoretical-Models. *Macromolecules* **1991**, *24*, 4481–4488, DOI: 10.1021/ma00016a001.

(70) Akcasu, A. Z.; Tombakoglu, M. Dynamics of Copolymer and Homopolymer Mixtures in Bulk and in Solution via the Random Phase Approximation. *Macromolecules* **1990**, *23*, 607–612, DOI: 10.1021/ma00204a038.

(71) Brereton, M. G.; Vilgis, T. A. Compatibility and Phase-Behavior in Charged Polymer Systems and Ionomers. *Macromolecules* **1990**, *23*, 2044–2049, DOI: 10.1021/ma00209a028.

(72) Benoit, H.; Benmouna, M.; Wu, W. L. Static Scattering from Multicomponent Polymer and Copolymer Systems. *Macromolecules* **1990**, *23*, 1511–1517, DOI: 10.1021/ma00207a045.

(73) Kudlay, A. N.; Erukhimovich, I. Y.; Khokhlov, A. R. Microphase Separation in Weakly Charged Annealed Gels and Associating Polyelectrolyte Solutions. *Macromolecules* **2000**, *33*, 5644–5654, DOI: 10.1021/ma992096r.

(74) Tanaka, F.; Ishida, M.; Matsuyama, A. Theory of Microphase Formation in Reversibly Associating Block Copolymer Blends. *Macromolecules* **1991**, *24*, 5582–5589, DOI: 10.1021/ma00020a016.

(75) Feng, E. H.; Lee, W. B.; Fredrickson, G. H. Supramolecular Diblock Copolymers: A Field-Theoretic Model and Mean-Field Solution. *Macromolecules* **2007**, *40*, 693–702, DOI: 10.1021/ma061653o.

(76) Lee, W. B.; Elliott, R.; Katsov, K.; Fredrickson, G. H. Phase Morphologies in Reversibly Bonding Supramolecular Triblock Copolymer Blends. *Macromolecules* **2007**, *40*, 8445–8454, DOI: 10.1021/ma071714y.

(77) Elliott, R.; Fredrickson, G. H. Supramolecular Assembly in Telechelic Polymer Blends. *J. Chem Phys.* **2009**, *131*, 144906, DOI: 10.1063/1.3244642.

(78) Man, X.; Delaney, K. T.; Villet, M. C.; Orland, H.; Fredrickson, G. H. Coherent States Formulation of Polymer Field Theory. *J. Chem. Phys.* **2014**, *140*, 024905, DOI: 10.1063/1.4860978.

(79) Read, D. J. Mean-Field Theory for Phase Separation During Polycondensation Reactions and Calculation of Structure Factors for Copolymers of Arbitrary Architecture. *Macromolecules* **1998**, *31*, 899–911, DOI: 10.1021/ma970953q.

(80) Benoit, H.; Hadziioannou, G. Scattering Theory and Properties of Block Copolymers with Various Architectures in the Homogeneous Bulk State. *Macromolecules* **1988**, *21*, 1449–1464, DOI: 10.1021/ma00183a040.

(81) Wittmer, J. P.; Milchev, A.; Cates, M. E. Dynamical Monte Carlo Study of Equilibrium Polymers: Static Properties. *J. Chem. Phys.* **1998**, *109*, 834–845, DOI: 10.1063/1.476623.

(82) Wittmer, J. P.; van der Schoot, P.; Milchev, A.; Barrat, J. L. Dynamical Monte Carlo Study of Equilibrium Polymers. II. The role of Rings. *J. Chem. Phys.* **2000**, *113*, 6992–7005, DOI: 10.1063/1.1311622.

(83) Loverde, S. M.; Ermoshkin, A. V.; de la Cruz, M. O. Thermodynamics of Reversibly Associating Ideal Chains. *J. Polym. Sci., Part B: Polym. Phys.* **2005**, *43*, 796–804, DOI: 10.1002/polb.20372.

(84) Benhamou, M.; Derouiche, A.; Bettachy, A. Microphase Separation of Cross-Linked Polymer Blends in Solution. *J. Chem. Phys.* **1997**, *106*, 2513–2519, DOI: 10.1063/1.473157.

(85) Bettachy, A.; Derouiche, A.; Benhamou, M.; Daoud, M. Phase-Separation of Weakly Cross-Linked Polymer Blends. *J. Phys. I* **1991**, *1*, 153–158, DOI: 10.1051/jp1:1991121.

(86) Benhamou, M. Field-Theoretical Approach to Critical Microphase Behavior of Symmetrical Cross-Linked Polymer Blends. *J. Chem. Phys.* **1995**, *102*, 5854–5862, DOI: 10.1063/1.469318.

(87) Stepanow, S.; Schulz, M.; Binder, K. Effects of Inhomogeneities of Cross-Links on a Microphase Separation of Polymer Mixtures. *J. Phys. II* **1994**, *4*, 819–824, DOI: 10.1051/jp2:1994166.

(88) Flory, P. J. Thermodynamics of High Polymer Solutions. *J. Chem. Phys.* **1942**, *10*, 51–61, DOI: 10.1063/1.1723621.

(89) Huggins, M. L. Theory of Solutions of High Polymers. *J. Am. Chem. Soc.* **1942**, *64*, 1712–1719, DOI: 10.1021/ja01259a068.

(90) Rubinstein, M.; Colby, R. H. *Polymer Physics*; Oxford University Press: New York, 2003.

(91) Hsu, C. C.; Prausnitz, J. M. Thermodynamics of Polymer Compatibility in Ternary-Systems. *Macromolecules* **1974**, *7*, 320–324, DOI: 10.1021/ma60039a012.

(92) Scott, R. L. Thermodynamics of High Polymer Solutions .VI. The Compatibility of Copolymers. *J. Polym. Sci.* **1952**, *9*, 423–432, DOI: 10.1002/pol.1952.120090504.

(93) Broseta, D.; Fredrickson, G. H. Phase-Equilibria in Copolymer Homopolymer Ternary Blends - Molecular-Weight Effects. *J. Chem. Phys.* **1990**, *93*, 2927–2938, DOI: 10.1063/1.458877.

(94) Scott, R. L. The Thermodynamics of High Polymer Solutions .V. Phase Equilibria in the Ternary System - Polymer-1 Polymer-2 Solvent. *J. Chem. Phys.* **1949**, *17*, 279–284, DOI: 10.1063/1.1747239.

(95) ten Brinke, G.; Karasz, F. E. Lower Critical Solution Temperature Behavior in Polymer Blends - Compressibility and Directional-Specific Interactions. *Macromolecules* **1984**, *17*, 815–820, DOI: 10.1021/ma00134a049.

(96) Sanchez, I. C.; Balazs, A. C. Generalization of the Lattice-Fluid Model for Specific Interactions. *Macromolecules* **1989**, *22*, 2325–2331, DOI: 10.1021/ma00195a056.

(97) Maconnachie, A.; Kambour, R. P.; White, D. M.; Rostami, S.; Walsh, D. J. Temperature-Dependence of Neutron-Scattering Behavior and Resultant Thermodynamics of Mixing of Poly(2,6-Dimethyl-1,4-Phenylene Oxide) in Polystyrene. *Macromolecules* **1984**, *17*, 2645–2651, DOI: 10.1021/ma00142a034.

(98) Hasegawa, H.; Sakurai, S.; Takenaka, M.; Hashimoto, T.; Han, C. C. Small-Angle Neutron-Scattering and Light-Scattering-Studies on the Miscibility of Protonated Polyisoprene/Deuterated Polybutadiene Blends. *Macromolecules* **1991**, *24*, 1813–1819, DOI: 10.1021/ma00008a019.

(99) Kim, E.; Kramer, E. J.; Osby, J. O.; Walsh, D. J. Mutual Diffusion and Thermodynamics in the Blends of Polystyrene and Tetramethylbisphenol-a Polycarbonate. *J. Polym. Sci. B: Polym. Phys.* **1995**, *33*, 467–478, DOI: 10.1002/polb.1995.090330315.

(100) Callaghan, T. A.; Paul, D. R. Interaction Energies for Blends of Poly(methyl methacrylate), Polystyrene, and Poly(alpha-methylstyrene) by the Critical Molecular-Weight Method. *Macromolecules* **1993**, *26*, 2439–2450, DOI: 10.1021/ma00062a008.

(101) Chu, J. H.; Paul, D. R. Interaction Energies for Blends of SAN with Methyl Methacrylate Copolymers with Ethyl Acrylate and n-Butyl Acrylate. *Polymer* **1999**, *40*, 2687–2698, DOI: 10.1016/S0032-3861(98)00499-6.

(102) Harada, M.; Suzuki, T.; Ohya, M.; Kawaguchi, D.; Takano, A.; Matsushita, Y. Novel Miscible Polymer Blend of Poly(4-trimethylsilylstyrene) and Polyisoprene. *Macromolecules* **2005**, *38*, 1868–1873, DOI: 10.1021/ma048527+.

(103) Hornreich, R. M.; Luban, M.; Shtrikman, S. Critical Behavior at Onset of **k**-Space Instability on λ-Line. *Phys. Rev. Lett.* **1975**, *35*, 1678–1681, DOI: 10.1103/PhysRevLett.35.1678.

(104) Bates, F. S.; Maurer, W. W.; Lipic, P. M.; Hillmyer, M. A.; Almdal, K.; Mortensen, K.; Fredrickson, G. H.; Lodge, T. P. Polymeric Bicontinuous Microemulsions. *Phys. Rev. Lett.* **1997**, *79*, 849–852, DOI: 10.1103/PhysRevLett.79.849.

(105) Hickey, R. J.; Gillard, T. M.; Irwin, M. T.; Lodge, T. P.; Bates, F. S. Structure, Viscoelasticity, and Interfacial Dynamics of a Model Polymeric Bicontinuous Microemulsion. *Soft Matter* **2016**, *12*, 53–66, DOI: 10.1039/c5sm02009c.

(106) Hillmyer, M. A.; Maurer, W. W.; Lodge, T. P.; Bates, F. S.; Almdal, K. Model Bicontinuous Microemulsions in Ternary Homopolymer Block Copolymer Blends. *J. Phys. Chem. B* **1999**, *103*, 4814–4824, DOI: 10.1021/jp990089z.

(107) Zhang, B.; Xie, S. Y.; Lodge, T. P.; Bates, F. S. Phase Behavior of Diblock Copolymer–Homopolymer Ternary Blends with a Compositionally Asymmetric Diblock Copolymer. *Macromolecules* **2021**, *54*, 460–472, DOI: 10.1021/acs.macromol.0c01745.

(108) Matsen, M. W. Stabilizing New Morphologies by Blending Homopolymer with Block-Copolymer. *Phys. Rev. Lett.* **1995**, *74*, 4225–4228, DOI: 10.1103/PhysRevLett.74.4225.

(109) Matsen, M. W.; Bates, F. S. Origins of Complex Self-Assembly in Block Copolymers. *Macromolecules* **1996**, *29*, 7641–7644, DOI: 10.1021/ma960744q.

(110) Bates, F. S.; Hillmyer, M. A.; Lodge, T. P.; Bates, C. M.; Delaney, K. T.; Fredrickson, G. H. Multiblock Polymers: Panacea or Pandora's Box? *Science* **2012**, *336*, 434–440, DOI: 10.1126/science.1215368.

(111) Prasad, I.; Jinnai, H.; Ho, R. M.; Thomas, E. L.; Grason, G. M. Anatomy of Triply-Periodic Network Assemblies: Characterizing Skeletal and Inter-domain Surface Geometry of Block Copolymer Gyroids. *Soft Matter* **2018**, *14*, 3612–3623, DOI: 10.1039/c8sm00078f.

(112) Buchanan, N.; Browka, K.; Ketcham, L.; Le, H.; Padmanabhan, P. Conformational and Topological Correlations in Non-Frustated Triblock Copolymers with Homopolymers. *Soft Matter* **2021**, *17*, 758–768, DOI: 10.1039/d0sm01612h.

(113) Leibler, L. Theory of Microphase Separation in Block Co-Polymers. *Macromolecules* **1980**, *13*, 1602–1617, DOI: 10.1021/ma60078a047.

(114) Dobrynin, A. V.; Erukhimovich, I. Y. Fluctuation Effects in the Theory of Weak Supercrystallization in Block Copolymer Systems of Complicated Chemical-Structure. *J. Phys. II* **1991**, *1*, 1387–1404, DOI: 10.1051/jp2:1991147.

(115) de la Cruz, M. O.; Sanchez, I. C. Theory of Microphase Separation in Graft and Star Copolymers. *Macromolecules* **1986**, *19*, 2501–2508, DOI: 10.1021/ma00164a008.

(116) von der Heydt, A.; Zippelius, A. Phase Diagram of Selectively Cross-Linked Block Copolymers Shows Chemically Microstructured Gel. *J. Chem. Phys.* **2015**, *142*, 054901, DOI: 10.1063/1.4905831.

(117) Derouiche, A.; Bettachy, A.; Benhamou, M.; Daoud, M. Kinetics of Microphase Separation in Cross-Linked Polymer Blends. *Macromolecules* **1992**, *25*, 7188–7191, DOI: 10.1021/ma00052a018.

(118) Joanny, J. F.; Leibler, L.; Ball, R. Is Chemical Mismatch Important in Polymer-Solutions? *J. Chem. Phys.* **1984**, *81*, 4640–4656, DOI: 10.1063/1.447399.

(119) Broseta, D.; Leibler, L.; Joanny, J. F. Critical Properties of Incompatible Polymer Blends Dissolved in a Good Solvent. *Macromolecules* **1987**, *20*, 1935–1943, DOI: 10.1021/ma00174a041.

(120) Schäfer, L.; Lehr, U.; Kappeler, C. Higher-Order Calculations of the Renormalization-Group Flow for Multicomponent Polymer-Solutions. *J. Phys. I* **1991**, *1*, 211–233, DOI: 10.1051/jp1:1991125.

(121) Fredrickson, G. H.; Leibler, L. Theory of Block Copolymer Solutions: Nonselective Good Solvents. *Macromolecules* **1989**, *22*, 1238–1250, DOI: 10.1021/ma00193a040.

(122) Whitmore, M. D.; Noolandi, J. Theory of Phase-Equilibria in Block Copolymer–Homopolymer Blends. *Macromolecules* **1985**, *18*, 2486–2497, DOI: 10.1021/ma00154a024.

(123) Banaszak, M.; Whitmore, M. D. Self-Consistent Theory of Block Copolymer Blends—Selective Solvent. *Macromolecules* **1992**, *25*, 3406–3412, DOI: 10.1021/ma00039a015.

(124) Wald, C.; Goldbart, P. M.; Zippelius, A. Glassy Correlations and Microstructures in Randomly Cross-Linked Homopolymer Blends. *J. Chem. Phys.* **2006**, *124*, 214905, DOI: 10.1063/1.2200697.

(125) Panyukov, S.; Rubinstein, M. Stress-Induced Ordering in Microphase-Separated Multicomponent Networks. *Macromolecules* **1996**, *29*, 8220–8230, DOI: 10.1021/ma960721b.

(126) Uchida, N. Pattern Formation in Microphase-Separating Copolymer Gels. *J. Phys. Condens. Matter* **2004**, *16*, L21–L27, DOI: 10.1088/0953-8984/16/4/L01.

(127) Lay, S.; Sommer, J. U.; Blumen, A. Monte Carlo Study of the Microphase Separation of Cross-Linked Polymer Blends. *J. Chem. Phys.* **2000**, *113*, 11355–11363, DOI: 10.1063/1.1326910.

(128) Mester, Z.; Lynd, N. A.; Delaney, K. T.; Fredrickson, G. H. Phase Coexistence Calculations of Reversibly Bonded Block Copolymers: A Unit Cell Gibbs Ensemble Approach. *Macromolecules* **2014**, *47*, 1865–1874, DOI: 10.1021/ma4026114.

(129) Delaney, K. T.; Fredrickson, G. H. Recent Developments in Fully Fluctuating Field-Theoretic Simulations of Polymer Melts and Solutions. *J. Phys. Chem. B* **2016**, *120*, 7615–34, DOI: 10.1021/acs.jpcb.6b05704.

(130) Lennon, E. M.; Katsov, K.; Fredrickson, G. H. Free Energy Evaluation in Field-Theoretic Polymer Simulations. *Phys. Rev. Lett.* **2008**, *101*, 138302, DOI: 10.1103/PhysRevLett.101.138302.

(131) Benmouna, M.; Vilgis, T. A.; Daoud, M.; Benhamou, M. Scattering and Phase-Behavior of Cross-Linked Blends. *Macromolecules* **1994**, *27*, 1172–1176, DOI: 10.1021/ma00083a015.

(132) Daoud, M.; Cotton, J. P. Star Shaped Polymers—a Model for the Conformation and Its Concentration-Dependence. *J. Phys. (Paris)* **1982**, *43*, 531–538, DOI: 10.1051/jphys:01982004303053100.

(133) Semenov, A. N. Theory of Block-Copolymer Interfaces in the Strong Segregation Limit. *Macromolecules* **1993**, *26*, 6617–6621, DOI: 10.1021/ma00076a047.

(134) Matsen, M. W.; Bates, F. S. Unifying Weak- and Strong-Segregation Block Copolymer Theories. *Macromolecules* **1996**, *29*, 1091–1098, DOI: 10.1021/ma951138i.

(135) Buzza, D. M. A.; Hamley, I. W.; Fzea, A. H.; Moniruzzaman, M.; Allgaier, J. B.; Young, R. N.; Olmsted, P. D.; McLeish, T. C. B. Anomalous Difference in the Order–Disorder Transition Temperature Comparing a Symmetric Diblock Copolymer AB with its Hetero-Four-Arm Star Analog A_2B_2. *Macromolecules* **1999**, *32*, 7483–7495, DOI: 10.1021/ma9904060.

(136) Matsen, M. W.; Gardiner, J. M. Anomalous Domain Spacing Difference between AB Diblock and Homologous A_2B_2 Starblock Copolymers. *J. Chem. Phys.* **2000**, *113*, 1673–1676, DOI: 10.1063/1.481967.

(137) Glotzer, S. C.; Bansil, R.; Gallagher, P. D.; Gyure, M. F.; Sciortino, F.; Stanley, H. E. Physical Gels and Microphase Separation in Multiblock Copolymers. *Phys. A* **1993**, *201*, 482–495, DOI: 10.1016/0378-4371(93)90121-J.

(138) Klopper, A.; Svaneborg, C.; Everaers, R. Microphase Separation in Cross-Linked Polymer Blends. *Eur. Phys. J. E: Soft Matter Biol. Phys.* **2009**, *28*, 89–96, DOI: 10.1140/epje/i2008-10420-6.

(139) Benhamou, M.; El Fazni, A.; Bettachy, A.; Derouiche, A. Theory of Microphase Separation in Crosslinked Polymer Blends Immersed in θ-Solvent. *Eur. Phys. J. E* **2010**, *32*, 391–398, DOI: 10.1140/epje/i2010-10643-x.

(140) Mohan, A.; Elliot, R.; Fredrickson, G. H. Field-Theoretic Model of Inhomogeneous Supramolecular Polymer Networks and Gels. *J. Chem. Phys.* **2010**, *133*, 174903, DOI: 10.1063/1.3497038.

(141) Schneiderman, D. K.; Hillmyer, M. A. 50th Anniversary Perspective: There Is a Great Future in Sustainable Polymers. *Macromolecules* **2017**, *50*, 3733–3750, DOI: 10.1021/acs.macromol.7b00293.

(142) Brutman, J. P.; De Hoe, G. X.; Schneiderman, D. K.; Le, T. N.; Hillmyer, M. A. Renewable, Degradable, and Chemically Recyclable Cross-Linked Elastomers. *Ind. Eng. Chem. Res.* **2016**, *55*, 11097–11106, DOI: 10.1021/acs.iecr.6b02931.

(143) Fortman, D. J.; Brutman, J. P.; De Hoe, G. X.; Snyder, R. L.; Dichtel, W. R.; Hillmyer, M. A. Approaches to Sustainable and Continually Recyclable Cross-Linked Polymers. *ACS Sustain. Chem. Eng.* **2018**, *6*, 11145–11159, DOI: 10.1021/acssuschemeng.8b02355.

(144) Elling, B. R.; Dichtel, W. R. Reprocessable Cross-Linked Polymer Networks: Are Associative Exchange Mechanisms Desirable? *ACS Cent. Sci.* **2020**, *6*, 1488–1496, DOI: 10.1021/acscentsci.0c00567.

(145) Yoon, J.; Mathers, R. T.; Coates, G. W.; Thomas, E. L. Optically Transparent and High Molecular Weight Polyolefin Block Copolymers Toward Self-Assembled Photonic Band Gap Materials. *Macromolecules* **2006**, *39*, 1913–1919, DOI: 10.1021/ma0516642.

(146) Lee, W.; Yoon, J.; Thomas, E. L.; Lee, H. Dynamic Changes in Structural Color of a Lamellar Block Copolymer Photonic Gel during Solvent Evaporation. *Macromolecules* **2013**, *46*, 6528–6532, DOI: 10.1021/ma302557v.

(147) McKeown, N. B.; Budd, P. M. Polymers of Intrinsic Microporosity (PIMs): Organic

Materials for Membrane Separations, Heterogeneous Catalysis and Hydrogen Storage. *Chem. Soc. Rev.* **2006**, *35*, 675–683, DOI: 10.1039/b600349d.

(148) Jackson, E. A.; Hillmyer, M. A. Nanoporous Membranes Derived from Block Copolymers: From Drug Delivery to Water Filtration. *ACS Nano* **2010**, *4*, 3548–3553, DOI: 10.1021/nn1014006.

(149) Schuster, B. S.; Regy, R. M.; Dolan, E. M.; Ranganath, A. K.; Jovic, N.; Khare, S. D.; Shi, Z.; Mittal, J. Biomolecular Condensates: Sequence Determinants of Phase Separation, Microstructural Organization, Enzymatic Activity, and Material Properties. *J. Phys. Chem. B* **2021**, *125*, 3441–3451, DOI: 10.1021/acs.jpcb.0c11606.

(150) Webber, M. J.; Appel, E. A.; Meijer, E. W.; Langer, R. Supramolecular Biomaterials. *Nat. Mater.* **2016**, *15*, 13–26, DOI: 10.1038/Nmat4474.

(151) Mandal, A.; Clegg, J. R.; Anselmo, A. C.; Mitragotri, S. Hydrogels in the Clinic. *Bioeng. Transl. Med.* **2020**, *5*, e10158, DOI: 10.1002/btm2.10158.

(152) Schauser, N. S.; Seshadri, R.; Segalman, R. A. Multivalent Ion Conduction in Solid Polymer Systems. *Mol. Syst. Des. Eng.* **2019**, *4*, 263–279, DOI: 10.1039/c8me00096d.

(153) Jones, S. D.; Schauser, N. S.; Fredrickson, G. H.; Segalman, R. A. The Role of Polymer-Ion Interaction Strength on the Viscoelasticity and Conductivity of Solvent-Free Polymer Electrolytes. *Macromolecules* **2020**, *53*, 10574–10581, DOI: 10.1021/acs.macromol.0c02233.

(154) Paulsen, B. D.; Tybrandt, K.; Stavrinidou, E.; Rivnay, J. Organic Mixed Ionic–Electronic Conductors. *Nat. Mater.* **2020**, *19*, 13–26, DOI: 10.1038/s41563-019-0435-z.